9
Polynuclear Coordination Cages

Michael D. Ward

9.1
Introduction

In the last couple of decades, the development of self-assembly methods in transition metal coordination chemistry has led to a large number of beautiful structures of a complexity which would previously have been inconceivable. From the first examples such as simple helicates in the 1980s [1,2] and small molecular grids in the 1990s [3,4], the repertoire of structural types that is accessible from a combination of polydentate bridging ligands and kinetically labile metal ions has expanded to include cages [5–7], rings [8,9], cylinders [10] and interlocked systems such as catenates [11,12] and knots [13]. Many of the first examples were the result of serendipity, however, there are equally many cases where the structures were the result of careful design and an understanding of how the geometric properties of a particular ligand would combine with the stereoelectronic preferences of a specific metal ion to yield the desired result.

One area which has been of particular recent interest is that of the preparation of polyhedral coordination cages. These compounds are attractive for several reasons. Their high-symmetry architectures have been of aesthetic interest and fascination since Plato first described the regular polyhedral solids (tetrahedron, octahedron, cube, dodecahedron and icosahedron), and it is no accident that such structures arise from self-assembly processes in nature in areas as superficially disparate as solid-state chemistry and biology [14,15]. Their high symmetry means that such structures can be particularly susceptible to rational design and there are many beautiful examples of polyhedral cage complexes in which careful matching of the symmetry properties of metal ions and rigid ligands whose geometric properties are fairly inflexible, have resulted in the planned synthesis of new cage architectures. The work of the groups of Raymond [5], Fujita [6] and Stang [7] is particularly notable in this regard. Finally, the fact that such cage complexes have – by definition – large central cavities means that they display intriguing host–guest chemistry, which at its simplest involves incorporation of solvent molecules or counter-ions and at its most sophisticated allows the cages to be used as "microreactors" in which new reactions can be catalyzed and hitherto inaccessible molecules stabilized [5,6].

Organic Nanostructures. Edited by Jerry L. Atwood and Jonathan W. Steed

ISBN: 978-3-527-31836-0

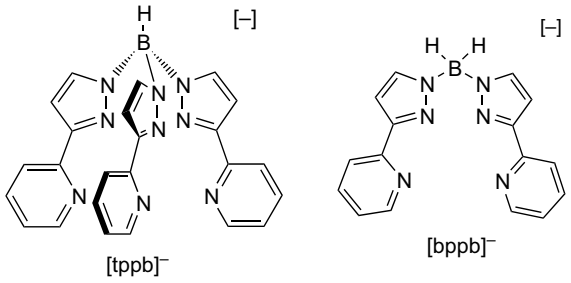

Scheme 9.1

This chapter presents a personal account of work in the author's research group over the last decade, in which relatively simple ligands based on bidentate pyrazolylpyridine chelating groups have been used as the basis for assembly of polyhedral cages. These ligands were originally developed as second-generation tris(pyrazolyl) borates in which the addition of 2-pyridyl groups to the pyrazolyl rings resulted in a hexadentate binding pocket in the ligand $[tppb]^-$ (Scheme 9.1) [16]. However, it quickly became apparent that this deceptively simple ligand had coordination behavior that was more complicated than we had anticipated and we consequently developed a series of ligands (Scheme 9.2) in which two or three of the bidentate

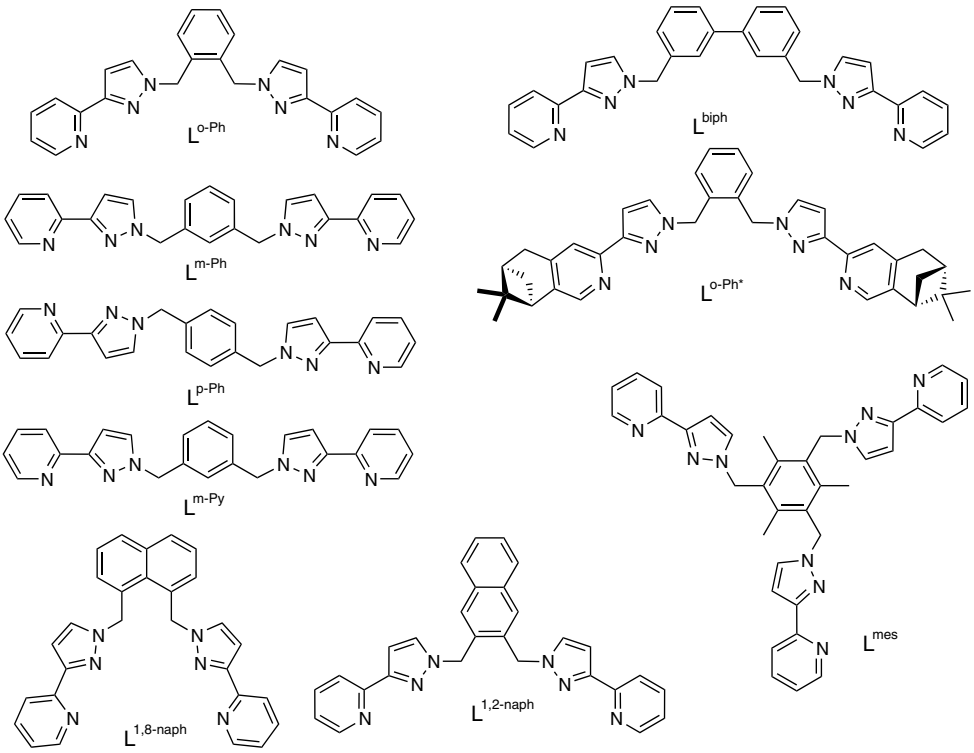

Scheme 9.2

pyrazolylpyridine groups were connected to organic spacers, which are resistant to the hydrolysis that occasionally plagues tris(pyrazolyl)borate chemistry. Serendipity has been a constant ally during this work. The ligands shown in Scheme 9.2 are inherently highly flexible because of the presence of saturated methylene spacers between the pyrazolylpyridine groups and the aromatic spacers, which were introduced for ease of synthesis. This precludes any possibility of control of the relative orientation of the binding sites and consequent deliberate design and synthesis of polyhedral cages, but it has resulted in many surprises, with many examples of unusual high-nuclearity cage structures appearing whose complexity is such that they could never, realistically, have been rationally designed.

9.2
Complexes Based on Poly(pyrazolyl)borate Ligands

Reaction of 3(2-pyridyl)pyrazole with KBH_4 readily afforded the bis- or tris(pyrazolyl) borate ligands $[bppb]^-$ or $[tppb]^-$ (Scheme 9.1) according to the stoichiometry and reaction temperature [16,17]. These ligands were originally planned as tetradentate or hexadentate chelates, respectively, for lanthanide(III) ions and indeed acted in this capacity perfectly well, generating an extensive series of complexes whose photophysical properties we studied [18].

With first-row transition metal ions, however, more complicated behavior emerged. Thus $[bppb]^-$ could act as a tetradentate chelate to lanthanide(III) ions and generate simple mononuclear complexes [18], but it could also act as a bridging ligand spanning two metal ions, which resulted in the unexpected formation of the octanuclear cyclic helicate $[Co_8(\mu\text{-bppb})_{12}(ClO_4)]^{3+}$ (Figure 9.1), whose assembly

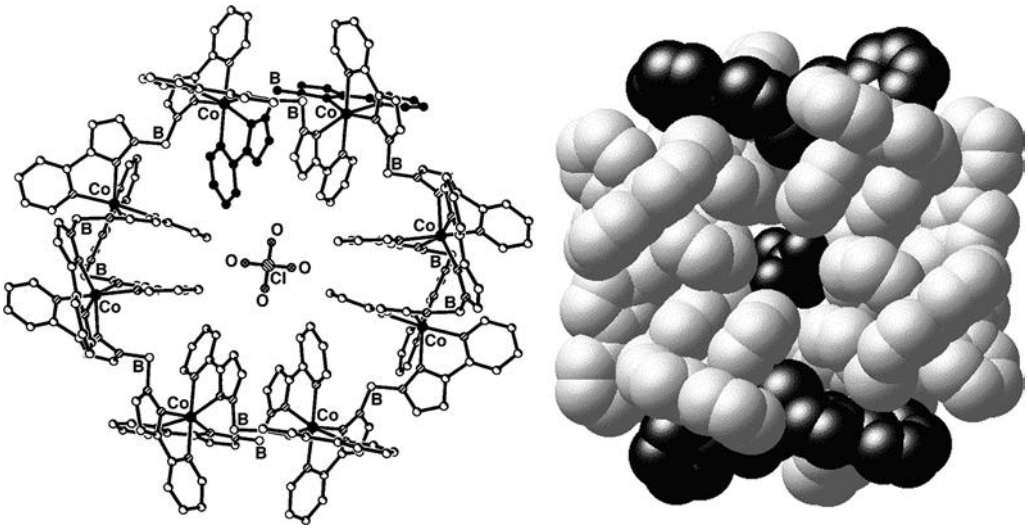

Figure 9.1 The complex cation of the cyclic octanuclear helicate $[Co_8(\mu\text{-bppb})_{12}(ClO_4)](ClO_4)_3$.

appears to be templated by the central perchlorate anion, which is a good fit for the central cavity [19]. The metal:ligand ratio of 2:3 is significant and a point that will be returned to later; it arises, necessarily, from the combination of a metal ion having a preference for octahedral coordination with a ligand which has four donor atoms. Thus, in the absence of coordinating anions or solvent molecules, 1.5 ligands are necessary to satisfy each metal ion, giving a stoichiometry of M_2L_3 or some higher multiple thereof.

The hexadentate ligand $[tppb]^-$ proved equally unpredictable (Figure 9.2). Its Co(II) complex $[Co(tppb)]^+$ is mononuclear with the metal ion in a rather unusual trigonal prismatic coordination geometry which is imposed by the ligand [20]; for this ligand to provide an octahedral coordination environment would require a high degree of twisting such that the N_3 plane provided by the pyridyl donors was staggered with respect to the N_3 plane provided the pyrazolyl donors. Clearly, it is not worth the cost in this complex. However, with metal ions such as Zn(II) and Mn(II), tetrahedral cages

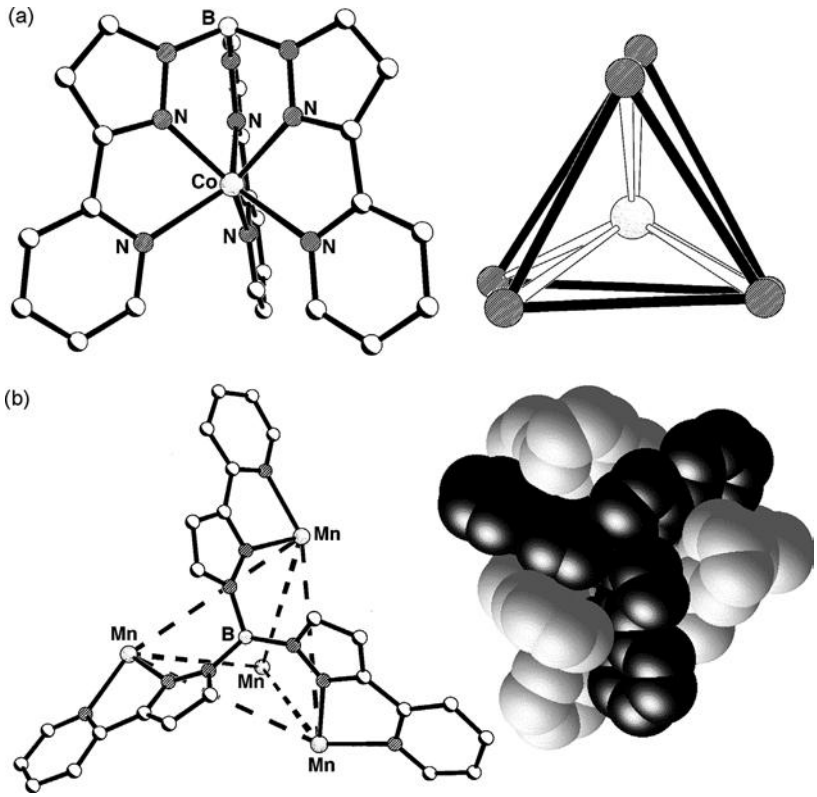

Figure 9.2 (a) The monomeric complex cation $[Co(tppb)]^+$, with trigonal-prismatic coordination of the metal ion; (b) the tetrameric complex cation $[Mn_4(tppb)_4]^{4+}$, with pseudo-octahedral coordination of the metal ion.

$[M_4(tppb)_4]^{4+}$ arise in which the ligand coordinates each of its three arms to a separate metal ion, effectively capping one face of an M_4 tetrahedron [20,21]. This previously unseen coordination mode for a tris(pyrazolyl)borate allows each metal ion, which interacts with three different ligands, to adopt an approximately octahedral coordination geometry that cannot be provided by one ligand alone. This pair of complexes provides a nice demonstration of how different stereoelectronic requirements of metal ions exerts a controlling influence on the course of the metal–ligand self-assembly process. A feature of the tetrahedral structure which may be significant in stabilizing it is the presence of aromatic π-stacking between overlapping aromatic rings of different ligands.

9.3
Complexes Based on Neutral Ligands with Aromatic Spacers

Following the above results, we prepared the simple bridging ligands shown in Scheme 9.2, in which an aromatic spacer is used instead of a borate group to connect the two pyrazolylpyridine chelates. The syntheses of these are straightforward, requiring reaction of 3-(2-pyridyl)pyrazole under basic conditions with a bis(bromomethyl) aromatic compound, such as 1,2-$C_6H_4(CH_2Br)_2$, to give $L^{o\text{-}Ph}$. The ready availability of bis(bromomethyl) aromatic compounds allowed the preparation of many related examples.

9.3.1
Complexes Based on $L^{o\text{-}Ph}$ and $L^{12\text{-}naph}$

The simplest members of this series, $L^{o\text{-}Ph}$ and $L^{12\text{-}naph}$, are the only ones in which the two bidentate arms are close enough together to chelate to a single metal ion and, as we saw with $[bppb]^-$, the coordination mode of the ligand varies. With Cu(II), a range of simple mononuclear complexes form in which $L^{o\text{-}Ph}$ acts as a tetradentate chelate [22]. Cu(I), however, has a preference for pseudo-tetrahedral coordination with two mutually perpendicular bidentate units, which cannot be met by a single $L^{o\text{-}Ph}$ ligand. The result is bridging behavior of the ligand in the dinuclear double helicate $[Cu_2(L^{o\text{-}Ph})_2]^{2+}$ [22]. With six-coordinate metal ions a 2M:3L ratio must arise, as explained earlier, and it is here that unexpected self-assembly behavior arises. There are many ways in which a 2M:3L ratio can be realized in a complex, of which the best known is a dinuclear triple helicate in which three bis-bidentate ligands each span two metal ions. We found instead two alternative types of structure depending on the size of the metal ion and the nature of the counter-ion.

Reaction of $L^{o\text{-}Ph}$ or its structurally similar analogue $L^{12\text{-}naph}$ with either Co(II) or Zn(II) as their fluoroborate or perchlorate salts afforded in each case tetrahedral cages $[M_4L_6X]X_7$ ($M = Co, Zn$; $L = L^{o\text{-}Ph}$, $L^{12\text{-}naph}$; $X = BF_4$, ClO_4) in which a tetrahedral array of metal ions is connected by a bridging ligand along each edge [23–25] (Figure 9.3). Note that the 2M:3L required to complete the coordination around octahedral metal ions is perfectly met by a tetrahedron which has four vertices (metal ions) and six edges (bridging ligands). Each metal ion is therefore approximately

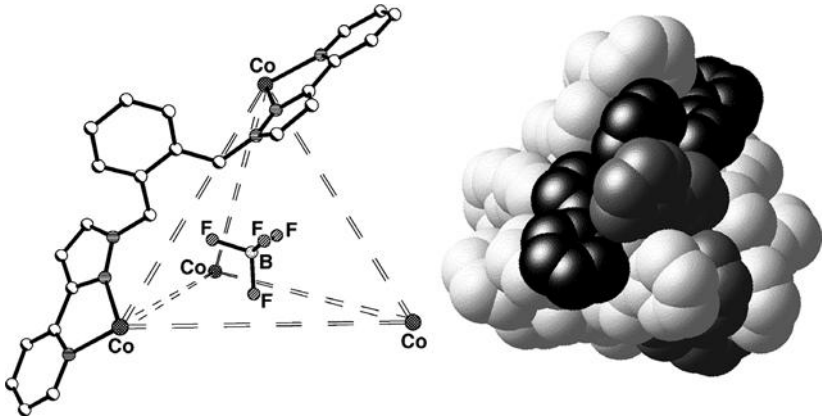

Figure 9.3 The tetranuclear cage complex cation of $[Co_4(L^{o\text{-}Ph})_6(BF_4)](BF_4)_7$, showing the tetrahedral superstructure with the encapsulated anion (left) and a space-filling picture emphasizing the close packing of ligands around the periphery (right).

octahedrally coordinated by one bidentate unit from each of three different ligands. In addition, several other features of these complexes are noteworthy:

1. The tetrahedral anion in the central cavity appears to be a perfect fit in terms of size, shape and charge. Each O atom (from perchlorate) or F atom (from tetrafluoroborate) occupies the space at the center of a triangular face of the tetrahedron, such that the tetrahedral anion is inverted with respect to the tetrahedral metal cage. The terminal O/F atoms interact with the cage superstructure via CH···O or CH···F hydrogen bonds with the CH_2 groups of the ligands. It is also clear from a space-filling view of the structures that the central anion is completely encapsulated by the metal–ligand cage, with no "windows" in the cage which would allow diffusion of the anions into or out of the cavity.

2. The structure is chiral, with all four metal centers having the same tris-chelate optical configuration; in fact the cage has (non-crystallographic) *T* symmetry with a C_3 axis through each vertex but no mirror planes. The crystals, however, are racemic with equal numbers of $\Delta\Delta\Delta\Delta/\Lambda\Lambda\Lambda\Lambda$ enantiomers in the unit cell.

3. There is extensive π-stacking between ligands around the cage involving overlap of aromatic groups between different ligands. This must provide some stabilization of the structure.

We return to each of these points in turn. The excellent fit of the perchlorate or tetrafluoroborate anion for the cage cavity, the involvement of the anion in hydrogen bonding to the cage superstructure and the complete encapsulation of the anions in every case all imply that the anion has acted as a template around which the cage assembles. Diffusion of an anion into a preformed but empty cage seems unlikely given the absence of "windows" in the cages. ^{19}F and ^{11}B NMR spectra on the fluoroborate-containing cages show the presence of two signals in a 7:1 ratio for the

external and encapsulated anions, respectively [23,25], and the spectra do not change significantly on warming up to the limit allowed by the solvent; thus any exchange of internal and external anions is slow on the NMR time-scale. That the central anion does act as a template was demonstrated conclusively by a simple ^{1}H NMR experiment on the Co(II) cages [24]. The paramagnetism of these cages shifts the ^{1}H NMR signals over a wide range between about −50 and 90 ppm and simple spectra were observed consistent with the high symmetry of the cages in solution, with all ligands equivalent and having twofold symmetry. In contrast a mixture of Co(II) acetate and $L^{o\text{-Ph}}$ or $L^{12\text{-naph}}$ in solution in the correct proportions (2:3) gave only a broad, ill-defined set of signals between 6 and 10 ppm. Addition of $NaBF_4$ or $NaClO_4$ to the NMR sample resulted in the immediate appearance of the characteristic simple, highly shifted set of peaks characteristic of the cage, which therefore only forms after addition of the tetrahedral anion which acts as a template for cage assembly.

The chirality of the cages makes them an appealing target to be resolved into their separate enantiomers. We have not yet been successful at this, but it is clear from NMR studies that diastereoisomers form in solution by ion pairing of the cage cations with the optically pure anion "trisphat" [tris(tetrachlorobenzenediolato)phosphate(V)] [26] . This results in some of the signals associated with the ligands in the ^{1}H spectrum splitting into two components (Figure 9.4) and – more intriguingly – results in the ^{19}F NMR signal for the encapsulated anion also splitting into two peaks with a separation of 2 ppm between the components arising from the two diastereoisomers (Figure 9.4). The chirality of the cage superstructure is therefore manifested through enantiodifferentiation of an achiral guest in the chiral cavity.

Since we could not separate the cage enantiomers by crystallization to get an optically pure sample, we adopted the alternative approach of adding a chiral auxiliary to the ligand ($L^{o\text{-Ph}^*}$, Scheme 9.2). The presence of two equivalent pinene

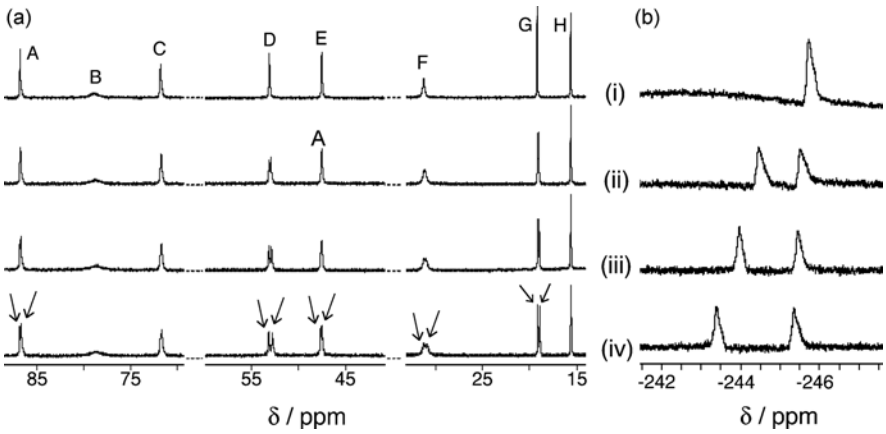

Figure 9.4 (a) 500-MHz ^{1}H NMR spectra and (b) 470-MHz ^{19}F NMR spectra of racemic $[Co_4(L^{o\text{-Ph}})_6(BF_4)](BF_4)_7$ in the presence of added portions of (i) 0, (ii) 2, (iii) 4 and (iv) 8 equiv. of (Bu_4N) (Δ-trisphat). Solvent: 5% CD_3NO_2 in $CDCl_3$.

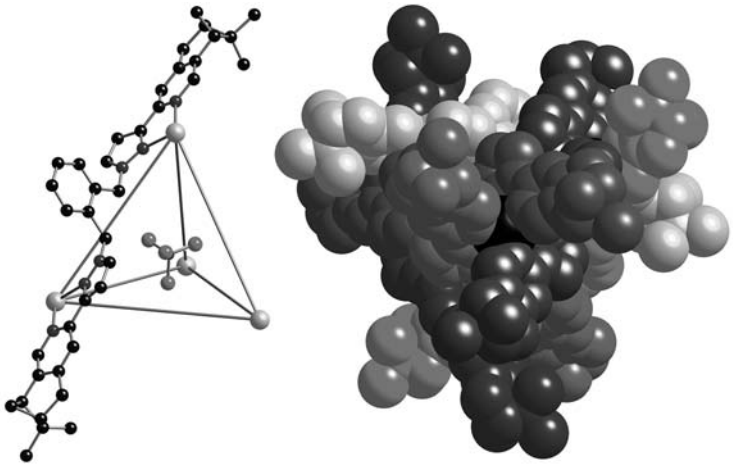

Figure 9.5 Two views of the optically pure cage complex $[Zn_4(L^{o\text{-}Ph^*})_6(ClO_4)](ClO_4)_7$: left, a view showing one ligand and the encapsulated anion; right, a space-filling picture viewed down a threefold rotation axis, showing the packing of the ligands.

substituents makes the ligand chiral, such that the two different forms of the cage – based on different tris-chelate configurations of the metal centers – would be diastereoisomers. The resulting cage complex $[Zn_4(L^{o\text{-}Ph^*})_6(ClO_4)](ClO_4)_7$ exists as a single diastereoisomer in solution, according to its ^1H NMR spectrum, and also crystallizes as a single diastereoisomer in the acentric space group C_2 (Figure 9.5) [27]. The specific molar rotation of this using 589-nm light is 30 times higher than the free ligand (13 400° in contrast to 432°). Given that the cage contains six ligands, it follows that there is an additional fivefold increase in the specific molar rotation arising from the fact that the chirality of the pinene groups on the ligands has dictated the chirality of the cage superstructure. Thus a set of six ligands undergoes a 500% amplification of specific molar rotation when the cage assembles and the ligands each adopt a helical twist; the magnitude of the molar rotation is comparable to those of compounds such as helicenes and a resolved trefoil knot.

The aromatic stacking between ligands around the periphery of the cage has significant consequences for the luminescence behavior of the Zn(II) cage based on $L^{12\text{-naph}}$. This ligand shows the characteristic fluorescence of the naphthyl group with an emission peak in the UV/blue region. In the cage $[Zn_4(L^{12\text{-naph}})_6][BF_4]_8$, however, the participation of the naphthyl group in aromatic stacking interactions with adjacent pyrazolylpyridine groups on either side of it lowers the energy of the emissive state in a manner similar to that seen in excimers (when two units of the same type stack together) to give an excited state that is delocalized over both. This results in red shifted, "excimer-like" luminescence from the naphthyl groups at about 440 nm in the cage compared to the free ligand $L^{12\text{-naph}}$ (Figure 9.6) [28]. The appearance of this red-shifted luminescence can be used as a probe to monitor cage formation in solution by the anion templation affect; titration of $NaBF_4$

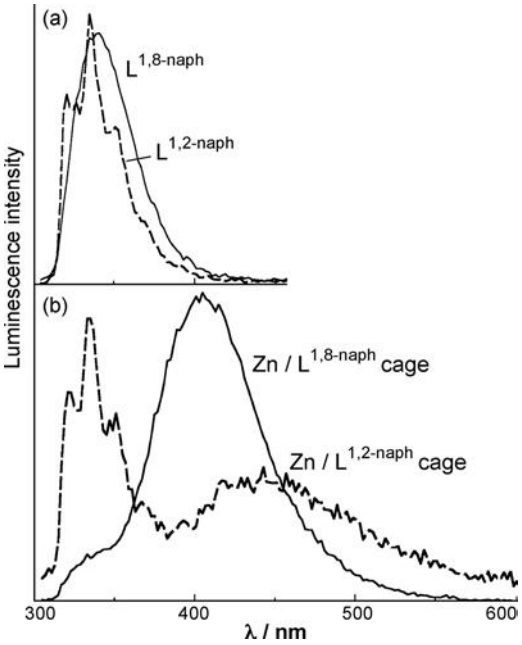

Figure 9.6 Naphthyl-based fluorescence of (a) free ligands $L^{12\text{-naph}}$ and $L^{18\text{-naph}}$ and (b) their tetranuclear and dodecanuclear (respectively) Zn(II) cages in which π-stacking of the naphthyl groups with other aromatic units results in red-shifted fluorescence.

into a mixture of Zn(II) acetate and $L^{12\text{-naph}}$ in solution results in a steady decrease in the intensity of the fluorescence associated with free $L^{12\text{-naph}}$ and the grow-in of the red-shifted fluorescence associated with aromatic stacking in the cage.

The highly intertwined structure of these cages results in remarkable kinetic stability. High-spin Co(II) centers are kinetically labile, as a simple demonstration shows [29]. $[Co(bipy)_3]^{2+}$ and $[Co(Me_2bipy)_3]^{2+}$ have, in their paramagnetically shifted ^1H NMR spectra, four and three aromatic signals, respectively, between 10 and 90 ppm. The signals for the aromatic protons that are in common between the two compounds [H(3), H(5), H(6)] have similar chemical shifts. When the two compounds are mixed in a 1:1 ratio, the resulting ^1H NMR spectrum – recorded as fast as possible after mixing, i.e. within about 2 min – is not a simple superposition of the two components, but shows that complete equilibration of the ligands between the metals has occurred with a statistical 1:3:3:1 mixture of $[CoA_3]^{2+}$, $[CoA_2B]^{2+}$, $[CoAB_2]^{2+}$ and $[CoB_3]^{2+}$. This is clearly shown by the presence of each of the H(3), H(5) and H(6) protons in eight environments with equal likelihood (one environment in each of the homoleptic complexes and three environments in each of the mixed-ligand complexes) (Figure 9.7). Thus in a mixture of kinetically labile $[Co(bipy)_3]^{2+}$-type complexes, ligand exchange is complete on a time-scale of a few minutes.

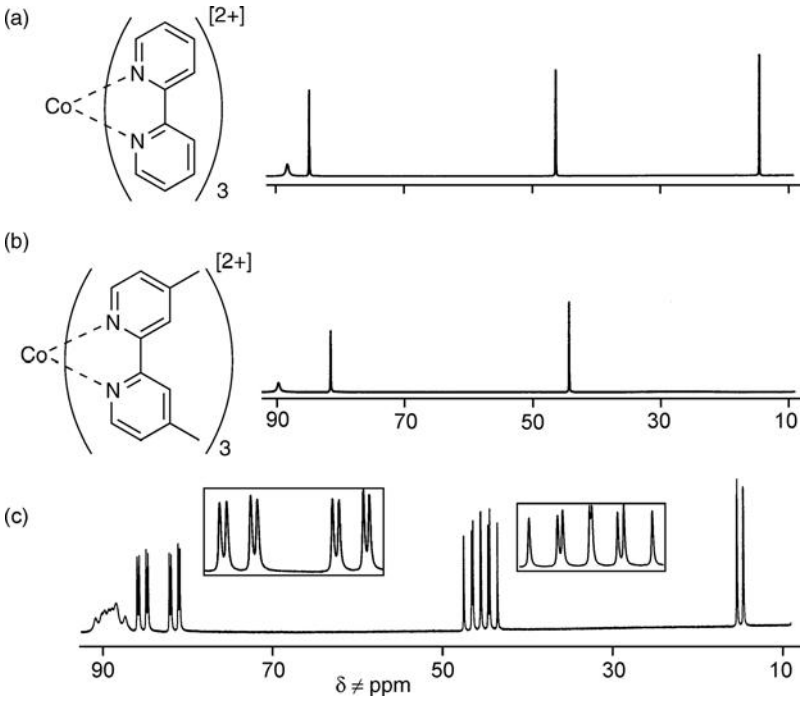

Figure 9.7 ^{1}H NMR spectra between 10 and 90 ppm of (a) $[Co(bipy)_3]^{2+}$, (b) $[Co(Me_2bipy)_3]^{2+}$ and (c) a 1:1 mixture of the above 2 min after mixing, showing a statistical equilibration of ligands between the metal ions.

In contrast, a 1:1 mixture of $[Co_4(L^{12\text{-naph}})_6(BF_4)][BF_4]_7$ and $[Co_4(L^{o\text{-Ph}})_6(BF_4)][BF_4]_7$, which have essentially identical structures, takes several *months* to reach equilibrium. The spectra of a 1:1 mixture of the complexes in the 10–90 ppm region are shown in Figure 9.8. The presence of two protons for the phenyl spacer versus three for the naphthyl spacer at around 20 ppm results in five signals in this region from simple superposition [spectrum (a)]; the remaining signals, arising from the pyrazolylpyridine groups and the methylene spacers, are almost identical between the two. If we abbreviate these complexes as Co_4A_6 and Co_4B_6 then at statistical equilibrium following ligand scrambling there should be seven species present: Co_4A_6, Co_4A_5B, $Co_4A_4B_2$, $Co_4A_3B_3$, $Co_4A_2B_4$, Co_4AB_5 and Co_4B_6. The simple 1:6:15:20:15:6:1 binomial distribution will be complicated by the fact that there could be two isomers for $Co_4A_4B_2$ and $Co_4A_2B_4$, according to whether the pair of ligands of the same type share a vertex or lie along opposed edges of the tetrahedron, and three isomers for $Co_4A_3B_3$. If all possible isomers exist at equilibrium then the mixture could contain up to 40 different environments for each type of proton.

After mixing, the ^{1}H NMR spectrum is just the sum of the two complexes, with no ligand scrambling evident. After several days, small additional peaks start to appear; after a couple of weeks they are fairly significant; after 3 months the spectrum stopped

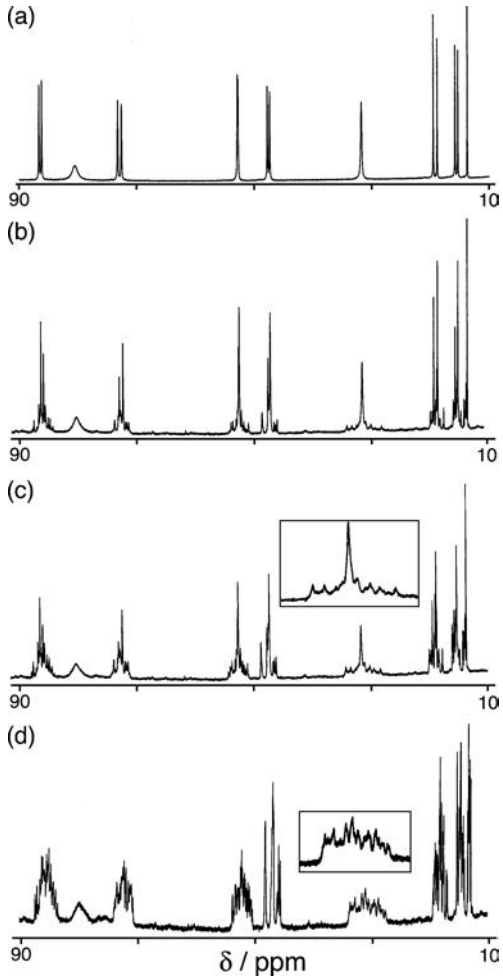

Figure 9.8 ^{1}H NMR spectra in CD_3CN between 10 and 90 ppm of a 1:1 mixture of $[Co_4(L^{12\text{-naph}})_6(BF_4)][BF_4]_7$ and $[Co_4(L^{o\text{-Ph}})_6(BF_4)][BF_4]_7$, at (a) 0, (b) 12, (c) 25 and (d) 79 days after mixing.

changing and it is clear that each type of proton now exists in a large number of different environments (Figure 9.8). Compared with the mononuclear $[Co(bipy)_3]^{2+}$ derivatives, it is obvious that formation of the tetrahedral cage assembly results in substantial kinetic stability, which will arise from several factors such as inter-ligand stacking interactions, hydrogen-bonding interactions with the central anion and the fact that the ligands are tetradentate rather than bidentate. All of these factors will inhibit dissociatively activated ligand exchange and the cumulative effect is substantial [29]. Raymond and coworkers have likewise noted remarkable kinetic inertness for some of their cages based on nominally labile metal centers [30].

Finally in this section, it should be pointed out that the formation of these cages between $L^{o\text{-Ph}}$ or $L^{12\text{-naph}}$ and Co(II) or Zn(II) is sensitive to the ionic radius of the

metal ion. Both Co(II) and Zn(II) have essentially the same ionic radius in octahedral coordination (89 pm); Ni(II), however, is significantly smaller (ionic radius in octahedral coordination, 83 pm) [31] and this prevents formation of the tightly packed cage complexes. Instead, reaction of $L^{o\text{-Ph}}$ or $L^{12\text{-naph}}$ with $Ni(BF_4)_2$ affords $[Ni_2L_3][BF_4]_4$. In these complexes, the necessary 2M:3L ratio is maintained, but in a simpler structure; each Ni(II) ion has one ligand (either $L^{o\text{-Ph}}$ or $L^{12\text{-naph}}$) acting as a tetradentate chelate occupying four of the six sites, with the remaining ligand acting as a bridge, donating one bidentate site to each Ni(II) ion. Even though the tetrafluoroborate anion is present the tetrahedral cages do not form, presumably because they would be too sterically crowded.

9.3.2
Larger Tetrahedral Cages Based on L^{biph}

We next used a biphenyl group as spacer, to make L^{biph}, with the intention of making similar tetrahedral cages but with larger cavities which might accommodate larger guest anions. Reaction of L^{biph} with a range of Co(II) salts afforded $[Co_4(L^{biph})_6X]X_7$ with a range of anions ($X^- =$ iodide, ClO_4^-, BF_4^-, PF_6^-), all of which were structurally characterized (Figure 9.9) [32]. Although these cages have the same basic topology as the smaller ones described in the previous section, there are important differences.

These cages no longer have *T* symmetry, because one vertex (nominally the apical one) has a *fac* tris-chelate configuration, whereas the three in the basal plane have a *mer* tris-chelate configuration. Hence there is only one (non-crystallographic) C_3 axis, through the apex. Accordingly, one-third of the complex is unique, with two independent ligand environments (apex-to-base and along the edges of the base), such that there are 44 inequivalent protons in the NMR spectrum. Not all of these are resolved but the paramagnetic shift effect of high-spin Co(II) spreads out the signals enough to make it clear that there are about this number of separate signals.

The longer ligands compared with $L^{o\text{-Ph}}$ or $L^{12\text{-naph}}$ result in a larger central cavity which accommodates equally well a range of anions of different sizes, the largest of which we have characterized to date is hexafluorophosphate. None of the anions used is a good match for the central cavity – all are too small to fill it effectively – which implies that a templating effect is unlikely to be operative. In addition, the anions are no longer completely encapsulated as there are windows in the centers of the triangular faces. In consequence, the internal anions are in fast exchange with the external ones at room temperature, with single signals appearing in the ^{19}F NMR spectra for both fluoroborate and hexafluorophosphate complexes. However, cooling results in the exchange becoming frozen out, with separate signals for the internal and external anions becoming apparent (Figure 9.9). From the linewidths of the ^{19}F NMR signals at different temperatures, we could estimate that the ΔG of activation for anion exchange is about 50 kJ mol^{-1} in each case [32]. This value suggests that the exchange mechanism involves diffusion of the anions through the windows of the intact cage; if the mechanism involved dissociation of a bidentate chelating group,

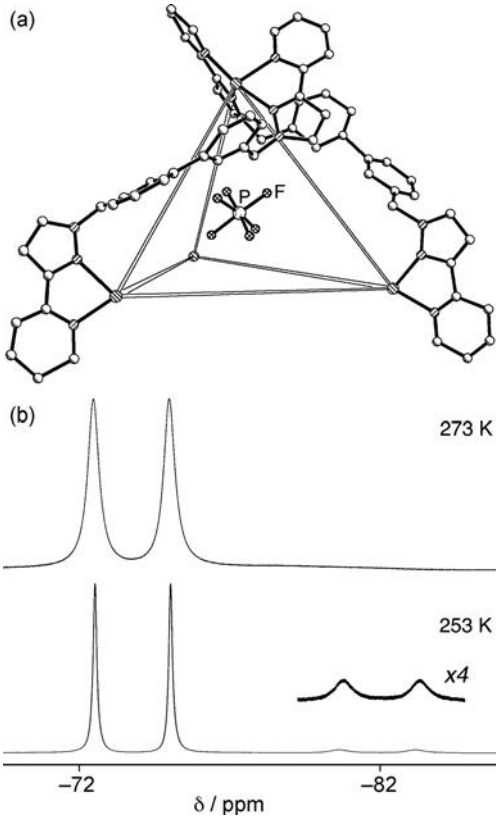

Figure 9.9 (a) Crystal structure of the complex cation of $[Co_4(L^{biph})_6(PF_6)](PF_6)_7$; (b) ^{19}F NMR spectra at different temperatures showing the "freezing out" of internal/external anion exchange (the doublets arise from coupling to ^{31}P of the hexafluorophosphate).

opening up the cage, the activation ΔG value would be higher as two Co–N bonds would have to break.

9.3.3
Higher Nuclearity Cages Based on Other Ligands

Additional simple changes to the ligands, by using different aromatic spacers between the pyrazolylpyridine arms, have afforded a series of unexpected high-nuclearity cages, all based on the simple 2:3 metal:ligand ratio, reflected in formation of polyhedra in which there is a 2:3 ratio of vertices (metal ions) to edges (bridging ligands).

Reaction of $L^{m\text{-}Ph}$ or $L^{m\text{-}Py}$ with Co(II) or Zn(II) salts affords molecular cubes $[M_8L_{12}]^{16+}$, with a metal ion at each vertex and a bridging ligand spanning each edge (Figure 9.10) [33,34]. In both cases the ligand coordinates in a bis-bidentate bridging

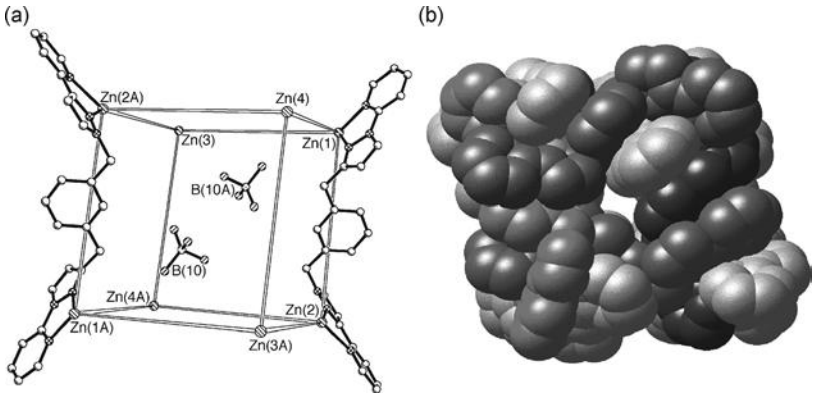

Figure 9.10 Crystal structures of the complex cations of (a) $[Zn_8(L^{m\text{-}Ph})_{12}][BF_4]_{16}$ (a view emphasizing the cubic array of metal ions and the encapsulated anions) and (b) $[Zn_8(L^{m\text{-}Py})_{12}](ClO_4)_{16}$ (a space-filling view).

manner; the central pyridyl unit of $L^{m\text{-}Py}$ does not participate in coordination [33], such that the pyridine–2,6-diyl spacer behaves just like the *m*-phenylene spacer of $L^{m\text{-}Ph}$ [34]. The cubes are slightly slanted, with angles at the corners in the range ca. 76–103°. The central cavity contains either one perchlorate anion, in $[Zn_8(L^{m\text{-}Py})_{12}](ClO_4)_{16}$, or two tetrafluoroborate anions, in $[Zn_8(L^{m\text{-}Ph})_{12}][BF_4]_{16}$; the windows in the centers of the faces, which are obvious in a space-filling representation of the structure, permit rapid exchange of internal and external anions as shown by ^{19}F NMR spectra of $[Zn_8(L^{m\text{-}Ph})_{12}][BF_4]_{16}$, for which a single signal occurs even at low temperatures.

The symmetry of these "cubic" cages is interesting. Unlike the tetrahedral cages, the tris-chelate metal centers in these cubes do not all have the same optical configuration, with a crystallographic inversion center lying at the center of the cube in each case such that the assemblies are achiral. There is a C_3 axis in each case lying along the long diagonal, with the two Zn(II) centers on this axis having a *fac* tris-chelate coordination and the others all having a *mer* geometry. The combination of a C_3 axis and an inversion center means that these cages actually have (non-crystallographic) S_6 symmetry. Extensive aromatic π-stacking between parallel, overlapping sections of ligands around the periphery of the complex is clear.

An additional and unexpected product which was isolated during the preparation of some of these cubic assemblies with $L^{m\text{-}Ph}$ is an "open-book" structure, exemplified by $[Co_6(L^{m\text{-}Ph})_9][ClO_4]_{12}$, which achieves the necessary 2:3 metal:ligand ratio in a different way (Figure 9.11) [34]. The assembly contains nine ligands associated with six octahedral metal ions; there are two $L^{m\text{-}Ph}$ ligands spanning each of the terminal pairs of Co(II) ions (the opposed open edges of the book – red and blue ligands in the figure) in a double helical arrangement, with all remaining Co—Co vectors (from each corner of the book to the spine and along the spine) having one bridging ligand. The two double helical sections are homochiral as they are related by a C_2 rotation

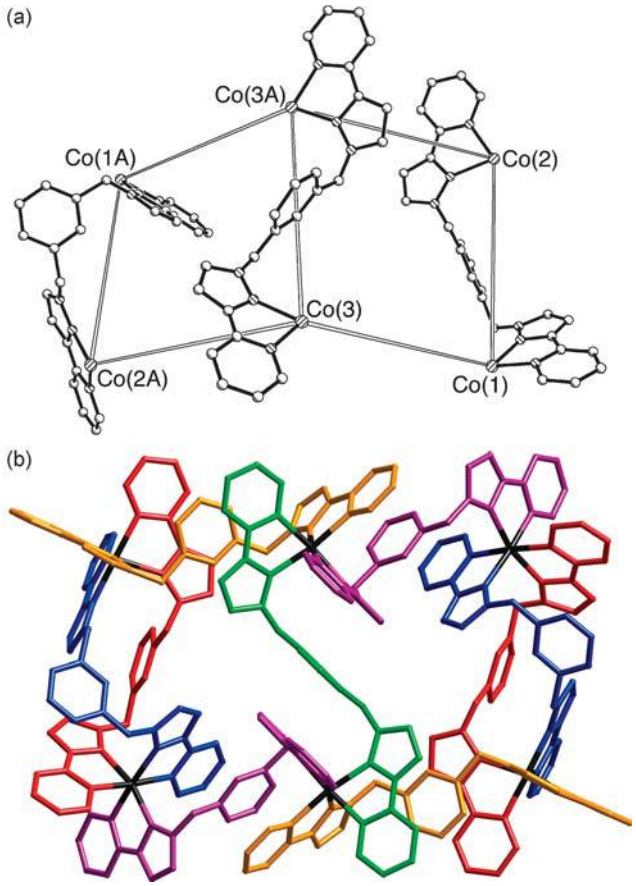

Figure 9.11 Two views of the crystal structure of the complex cation $[Co_6(L^{m\text{-}Ph})_9][ClO_4]_{12}$: (a) a view emphasizing the "open-book" arrangement of metal centers; (b) a view showing all of the ligands.

through the center of the complex. Although this complex is not in itself of great significance from the point of view of our investigations into polyhedral cages, it does illustrate how a single combination of a metal salt and a ligand can follow two different self-assembly pathways to give a mixture of different products which nevertheless obey the same basic stoichiometric principle of having a 2M:3L ratio.

Reaction of $L^{1,8\text{-naph}}$ with a range of M(II) ions [Cd(II), Co(II), Cu(II), Zn(II)] and either BF_4^- or ClO_4^- as counter-ion, affords $[M_{12}(L^{1,8\text{-naph}})_{18}]^{24+}$ cages having the core structure of a truncated tetrahedron (Figure 9.12) [35,36]. Slicing off the vertices of a notional tetrahedron generates four new triangular faces (shaded in the figure); the original triangular faces become hexagons when the vertices are removed. The truncated tetrahedral structure is the simplest of the series of Archimedean solids and conveniently provides 18 edges to go with the 12 vertices, in keeping with the

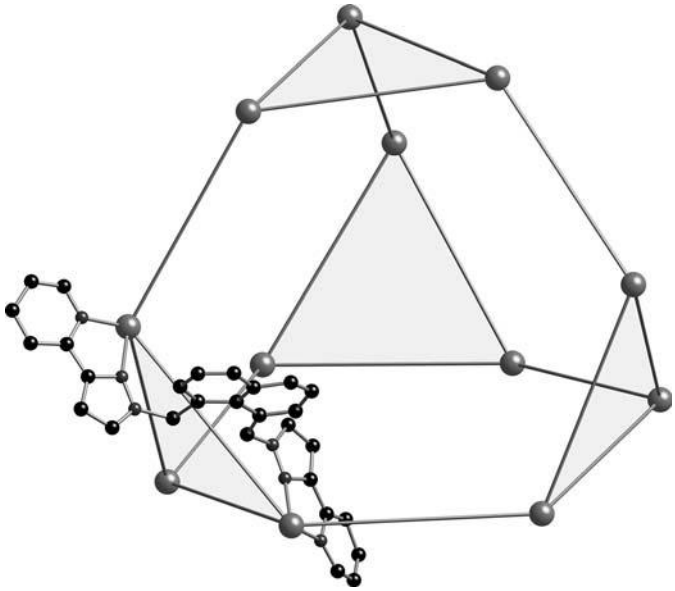

Figure 9.12 A view of the polyhedral metal core of $[Cu_{12}(L^{1,8\text{-naph}})_{18}](ClO_4)_{24}$; each edge of the polyhedron is spanned by a bridging ligand, of which one example is included. The four faces shaded gray are those derived from truncating the apices of a notional tetrahedron.

stoichiometric requirements; there is an M(II) ion at each vertex and a bridging ligand spanning each edge, connecting a pair of metal ions. Around each of the triangular and hexagonal faces the array of bridging ligands forms a cyclic helical structure (Figure 9.13).

It is not obvious why such a complex structure should form when there must be so many simpler alternatives with the same net number of metal–ligand interactions but higher entropy. One possibility is the stabilization afforded by extensive aromatic stacking between ligands around the periphery. Stacks of seven components – an alternating sequence of naphthyl and pyrazolylpyridine units in a seven-layer sandwich – occur, with six such stacks arranged in a roughly cubic array around the outside of the complex. As with the smaller tetranuclear cage based on $L^{1,2\text{-naph}}$, this involvement of the naphthyl groups in extensive aromatic

Figure 9.13 Three views of the structure of $[Cd_{12}(L^{naph})_{18}](BF_4)_{24}$: (a) a view of the polyhedral metal cage and the four encapsulated $[BF_4]^-$ anions; (b) a view down one of the triangular faces, emphasizing the cyclic helical array of ligands around the face and the presence of an anion in the center of the face; (c) a view down one of the Cd_6 pseudo-hexagonal faces, emphasizing the cyclic helical array of ligands around the face and the presence of an anion in the center of the face.

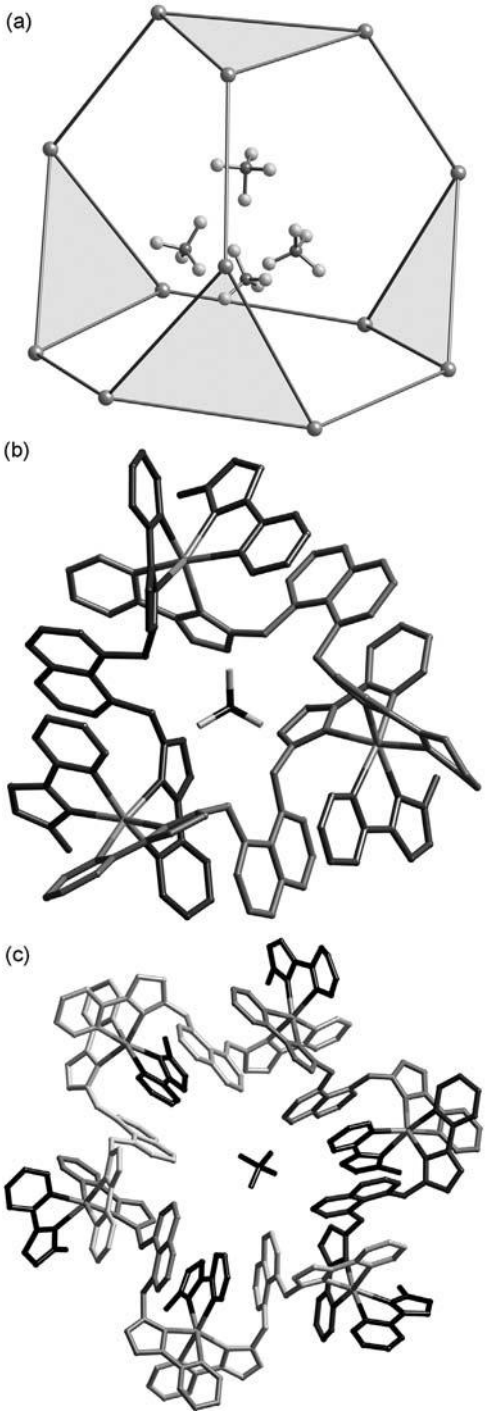
(a)
(b)
(c)

stacking stabilizes the fluorescent excited state of the ligands and results in strongly red-shifted luminescence from $[Zn_{12}(L^{1,8\text{-naph}})_{18}][BF_4]_{24}$ compared with free $L^{1,8\text{-naph}}$ (Figure 9.6) [28].

Two other features of these cages are noteworthy. First, the central cavity is now large enough to accommodate four BF_4^- or ClO_4^- anions. These are themselves disposed in a roughly tetrahedral array and are fairly close together with their peripheral atoms separated by about the sum of the van der Waals radii. Apparently the unfavorable anion–anion interactions between these four guest anions are more than offset by the electrostatic advantage of accommodating four anions in a cage superstructure with a charge of 24^+. There are also anions associated with the windows in the centers of the triangular and hexagonal faces (Figure 9.13); since there are eight faces, this makes a total of 12 anions closely associated with the 24^+ cage. Second, all 12 metal tris-chelate centers have the same optical configuration, which is necessary for the roughly spherical surface to achieve closure. Altering the configuration at any metal site would result in one of the ligands extending into space away from the core and unable to bridge to a second metal ion. Thus, 72 metal–ligand bonds have to form with the correct optical configuration during the cage assembly. The bulk material of course is racemic. The view on to each type of face (triangular or hexagonal) is that of a cyclic helicate; hence, looking down on a hexagonal face one sees that the six bridging ligands associated with that face have the "over and under" sequence characteristic of a cyclic helicate and the same is true of the set of three ligands associated with each triangular face.

The largest homoleptic cage that we have yet isolated was provided by reaction of $L^{p\text{-Ph}}$ with M(II) salts to give the hexadecanuclear cages $[M_{16}(L^{p\text{-Ph}})_{24}]X_{32}$ ($M = Zn$, $X = BF_4$; $M = Cd$, $X = ClO_4$) whose polyhedral core of metal ions may be approximately described as a tetra-capped truncated tetrahedron [37]. The structure of $[Cd_{16}(L^{p\text{-Ph}})_{24}](ClO_4)_{32}$ is shown as an example (Figures 9.14 and 9.15). Each apex of a tetrahedron is sliced off to reveal a triangular face; the resulting truncated tetrahedron has 12 vertices, with four triangular faces and four hexagonal faces, as described above. The four triangular faces are then twisted in the same sense, such that the mirror planes through the truncated tetrahedron are removed but the C_3 axes are retained. Finally, a capping atom is added to the center of each of the original four faces. This M_{16} polyhedral array, with (non-crystallographic) *T* symmetry, has a bridging ligand $L^{p\text{-Ph}}$ along each of the 24 edges, providing the necessary 2:3 $M:L^{p\text{-Ph}}$ ratio. The large central cavity contains eight $[ClO_4]^-$ anions and six MeCN molecules. In contrast to the behavior observed with much smaller cages, this is a very "open" structure with the anions clearly not completely encapsulated by the cage superstructure.

The Cd(II) centers display a mix of facial and meridional tris-chelate geometries; the 12 Cd(II) centers associated with the four triangular faces of the truncated tetrahedron have a meridional arrangement and the four "capping" metal centers are facial. Remarkably, and as we saw with the dodecanuclear truncated-tetrahedral complexes, all 16 metal centers have the same optical configuration, which appears to be essential for the closed cage to form; thus the assembly has occurred with correct

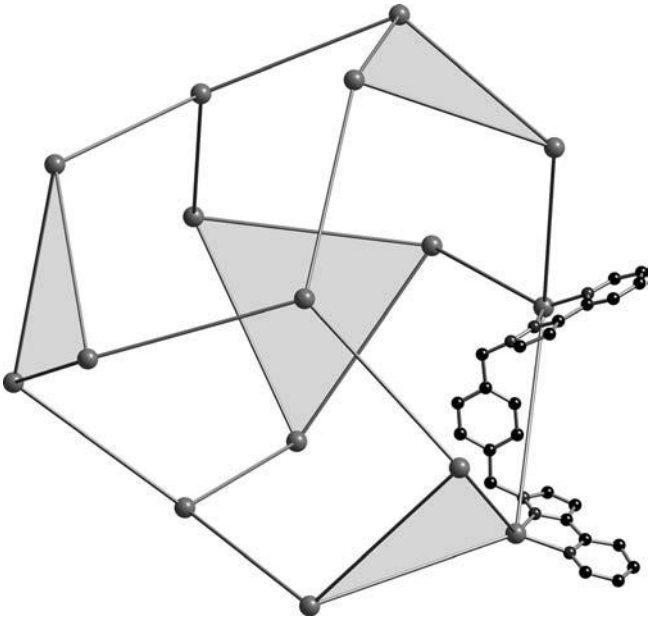

Figure 9.14 A view of the polyhedral metal core of $[Cd_{16}(\mu\text{-}L^{p\text{-}Ph})_{24}](ClO_4)_{32}$; each edge of the polyhedron is spanned by a bridging ligand, of which one example is included. The four faces shaded gray are those notionally derived from truncating the apices the parent tetrahedron.

control of 96 metal–ligand bonds. The crystal is racemic, containing equal numbers of opposite enantiomers of the cage.

So far, the polyhedral cages that we have observed to date based on these bis-bidentate pyrazolylpyridine ligands (M_4L_6 tetrahedron, Figures 9.3 and 9.9; M_8L_{12} cube, Figure 9.10; $M_{12}L_{18}$ truncated tetrahedron, Figure 9.12; $M_{16}L_{24}$ tetra-capped truncated tetrahedron, Figure 9.14) all necessarily contain a 2M:3L ratio as a result of combining octahedral metal ions (vertices) with bis-bidentate bridging ligands (edges). Clearly there could be an infinite number of possible larger structures which obey the same stoichiometric principle, although there must come a point at which the entropic cost becomes prohibitive. The prevalence of *T*-symmetry structures (observed for the M_4L_6, $M_{12}L_{18}$ and $M_{16}L_{24}$ cages) is interesting; Cotton et al. have pointed out that *T*-symmetric species may be derived in a wide variety of ways by "downgrading" assemblies with tetrahedral, octahedral or icosahedral symmetry by removal of mirror planes [38].

It is also important to emphasize the fact that crystals can grow under kinetic control and the structures may not represent thermodynamic minima in solution; there are many well-established examples in the field of self-assembly of transition metal complexes where a mixture of interconverting species in solution (a "dynamic combinatorial library") generates a single (kinetic) product on crystallization. We know for the smaller tetrahedral cages, from a combination

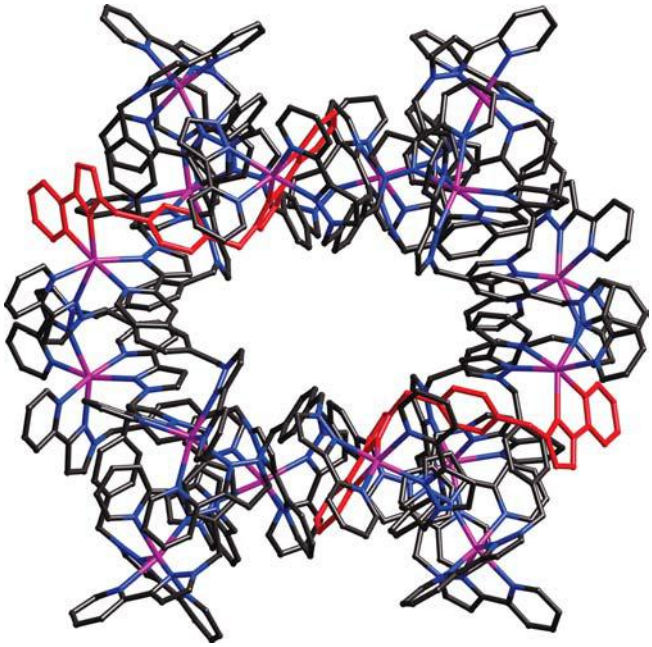

Figure 9.15 A view of $[Cd_{16}(\mu\text{-}L^{p\text{-}Ph})_{24}](ClO_4)_{32}$ showing all atoms in the cage, with two of the bridging ligands colored red (Cd, purple; N, blue).

of NMR and mass spectrometric studies, that the cage structures are retained in solution [23–25]. For the larger cages, it becomes even more important to use solution methods to confirm the existence of the cages in solution and electrospray mass spectrometry is an ideal tool (a ^{1}H NMR spectrum will not distinguish effectively between different metal–ligand assemblies, especially those based on diamagnetic metal cations where all of the signals of interest associated with the ligands come in a narrow range). Examples of an electrospray mass spectrum of one of the 12-nuclear cage complexes is shown in Figure 9.16; such spectra provide clear proof that the cage structures are retained *to some extent* in solution. The presence of smaller and simpler assemblies cannot be ruled out, however: a peak corresponding to the presence of a M_2L_3 assembly, for example, may arise from fragmentation of a larger cage – or it may genuinely correspond to the presence of a simple dinuclear complex as part of an equilibrium mixture. The presence of alternative metal–ligand assemblies has been unequivocally established in one case by isolation and structural characterization of both $[M_8(L^{m\text{-}Ph})_{12}]^{16+}$ and $[M_6(L^{m\text{-}Ph})_9]^{12+}$ complexes from the same metal–ligand combination [34]. The possibility to exploit these polyhedral cages as hosts for, e.g., size- or shape-selective anion binding will require kinetically inert cages which do not dissociate in solution. So far this behavior has only been established unequivocally for the series $[M_4L_6X]X_7$ (M = Co, Zn; L = $L^{o\text{-}Ph}$, $L^{12\text{-}naph}$; X = BF_4, ClO_4), in which

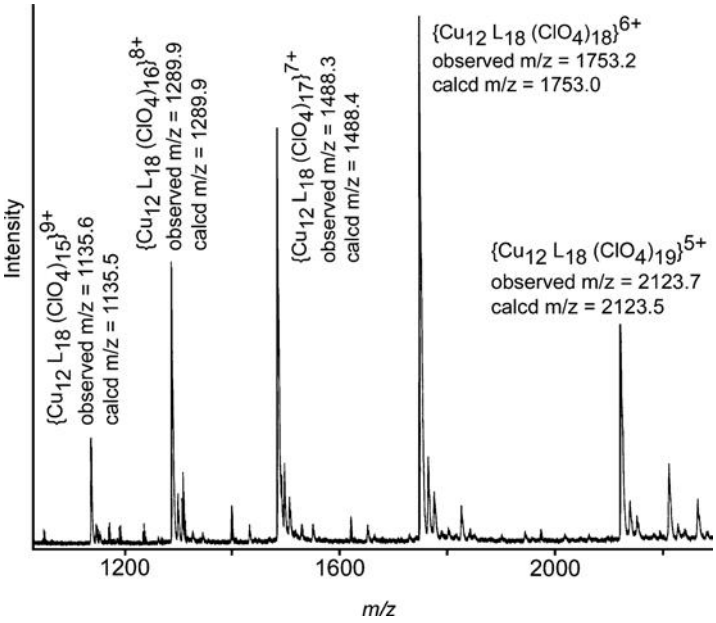

Figure 9.16 Part of the electrospray mass spectrum of $[Cu_{12}(L^{1,8\text{-naph}})_{18}](ClO_4)_{24}$ showing the intact cage with loss of 5, 6, 7, 8 and 9 perchlorate anions.

the anion exerts a templating effect and remains tightly bound in the central cavity even at elevated temperatures according to NMR spectra [23–25].

9.4
Mixed-ligand Complexes: Opportunities for New Structural Types

All of the above examples – and, indeed, most polynuclear coordination complexes formed by self-assembly methods – contain a single type of ligand. Using a mixture of ligands L^A and L^B in a reaction with a labile metal ion introduces a much higher degree of complexity to the problem. In addition to the possibilities that could arise from reaction of a metal ion with one ligand on its own, which (as we have seen above) are extensive and unpredictable, there is the additional possibility of mixed-ligand complexes occurring if there are any favorable interactions between L^A and L^B which make it likely that they will occur together in the same assembly. Notable examples of reactions in which a metal ion reacts with a specific combination of different ligands to generate a single mixed-ligand product are provided by (i) Lehn's cylindrical stacks which combine both linear bridging ligands along the edges and triangular tritopic bridging ligands in the core [39] and (ii) mixed-ligand rectangular grid complexes which form in preference to the homoleptic grids [40].

A simple illustration of the issues is provided by the bis-bidentate bridging ligands L^1 and L^2 which contain two *N,O*-chelating pyrazolylphenolate units (Scheme 9.3).

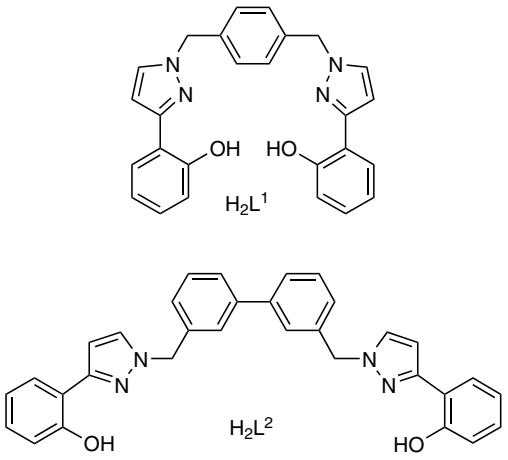

Scheme 9.3

These ligands both form simple dinuclear double helicates M_2L_2 with M = Cu and Zn in which each metal ion is four coordinate [41]. When $M_2(L^1)_2$ and $M_2(L^2)_2$ are mixed in a 1:1 ratio in solution there are three possible outcomes. First, the homoleptic complexes could remain as they are with no significant amounts of mixed-ligand complexes forming; this might happen if there were any unfavorable interactions between L^1 and L^2. If there were no significant interactions between L^1 and L^2 then we might expect a statistical mixture of $M_2(L^1)_2$, $M_2(L^1)(L^2)$ and $M_2(L^2)_2$ in a 1:2:1 ratio. If there were an attractive interaction between L^1 and L^2 then the mixed-ligand system would dominate and there would be relatively little of the homoleptic complexes. In these cases, with both Cu(II) and Zn(II), the mixed-ligand complexes $M_2(L^1)(L^2)$ dominate according to mass spectrometry and could be preferentially crystallized (Figure 9.17) [42]. The Cu(II) complex is a conventional double helicate, but contains in the solid state inter-ligand aromatic stacking interactions with the phenyl spacer of one ligand sandwiched between the two pyrazolylphenolate termini of the other. Since no such inter-ligand interactions were present in either of the homoleptic complexes $Cu_2(L^1)_2$ and $Cu_2(L^2)_2$ and there is no obvious electronic reason why two equivalents of $Cu_2(L^1)(L^2)$ should be preferred over a mixture of the homoleptic complexes, we suggest that this stacking plays a significant role in stabilizing the mixed-ligand helicate. In contrast the mixed-ligand Zn(II) complex $Zn_2(L^1)(L^2)$ is a "mesocate" with the two ligands in a side-by-side arrangement and not helically intertwined, unlike the parent helicates $Zn_2(L^1)_2$ and $Zn_2(L^2)_2$. The reason for preferential formation of the mixed-ligand Zn(II) complex compared with the homoleptic complexes is not obvious.

Two examples of mixed-ligand complexes which combine tetradentate and hexadentate bridging ligands show how new structural types, which are not accessible from either ligand on its own, can be isolated. The bis-bidentate bridging ligands form polyhedral arrays with metal cations in which the ligands span the *edges* of the polyhedron; in contrast the tris-bidentate ligands coordinate to three

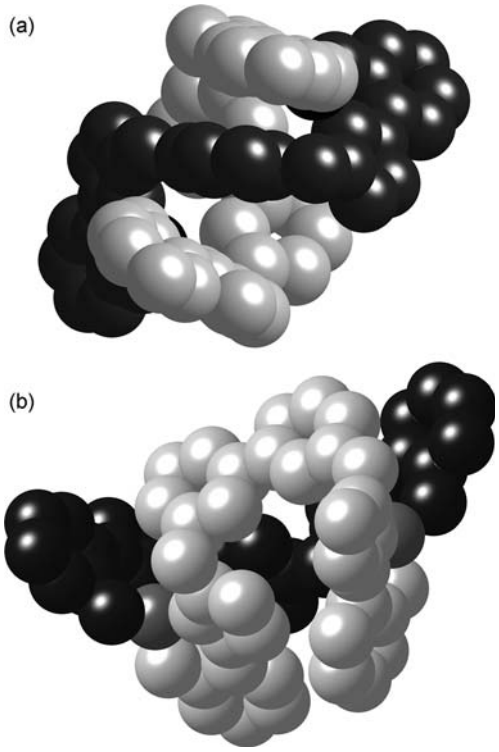

Figure 9.17 Structures of the mixed-ligand complexes $M(L^1)(L^2)$: (a) a double helicate with M = Cu; (b) a mesocate with M = Zn with the ligands in a "side-by-side" arrangement rather than helically twisted around one another.

metal ions at a time, capping the *faces* of the polyhedron, as shown in $[M_4(tppb)_4]^{4+}$ [20,21]. A mixture of the bis- and tris-pyrazolylborate ligands $[bppb]^-$ and $[tppb]^-$ reacts with Mn(II) to form, in addition to homoleptic complexes, the mixed-ligand trinuclear complex $[Mn_3(tppb)(bppb)_3]^{2+}$, a triangular complex with one face-capping $[tppb]^-$ ligand and three edge-bridging $[bppb]^-$ ligands (Figure 9.18) [43]. Clearly, such a structure could not arise in a homoleptic complex based on these components.

A more spectacular example based on the same principles is provided by reaction of $M(BF_4)_2$ (M = Cu, Zn, Cd) with a mixture of L^{mes} (a three-armed triangular ligand with a mesityl core) and $L^{p\text{-}Ph}$. {Recall that use of $L^{p\text{-}Ph}$ alone afforded the hexadecanuclear cages $[M_{16}(L^{p\text{-}Ph})_{24}]^{32+}$ with a 2:3 M:L ratio; we could not (yet) isolate a homoleptic complex with L^{mes} but it must have a 1:1 M:L ratio with an octahedral metal cation}. The crystalline products from these reactions are the mixed-ligand complexes $[M_{12}(\mu\text{-}L^{p\text{-}Ph})_{12}(\mu^3\text{-}L^{mes})_4](BF_4)_{24}$ (Figures 9.19 and 9.20) which has a cuboctahedral metal framework containing eight triangular and six square faces [37]. The complex lies on a C_2 axis. Four of the eight

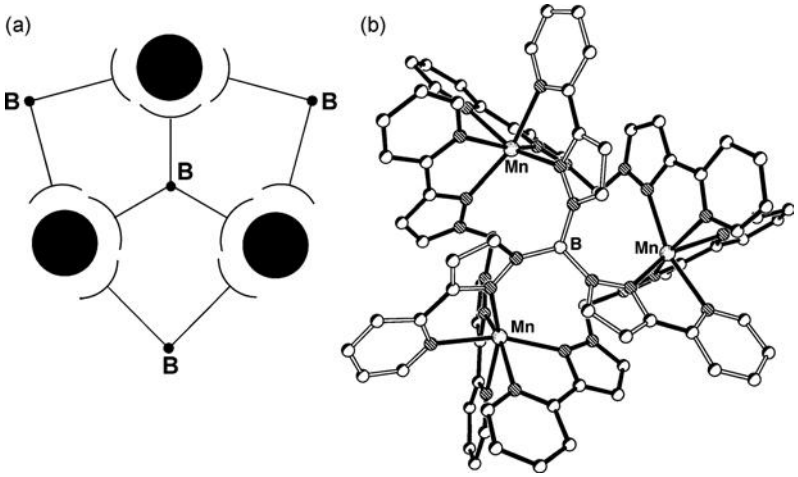

Figure 9.18 (a) A sketch showing how one face-capping (tris-bidentate) and three edge-bridging (bis-bidentate) ligands can afford a trinuclear valence-satisfied complex based on six-coordinate metal ions; (b) crystal structure of the complex cation $[Mn_3(tppb)(bppb)_3]^{2+}$ which conforms to this principle.

triangular faces are capped by a triply bridging ligand L^{mes} and the remaining vacant edges are spanned by twelve doubly bridging ligands $L^{p\text{-}Ph}$. Numerous counter-ions and solvent molecules occupy the open space in the center of the complex. It is interesting that the 1:3 ratio of face capping:edge bridging ligands in this complex is the same as was observed in the simpler complex $[Mn_3(tppb)(bppb)_3]^{2+}$.

All 12 tris-chelate metal centers have meridional geometry and again all have the same chirality, indicating that the same chiral configuration at each metal center is necessary for the closed cage to form. The crystal is racemic. In this case electrospray mass spectra on solutions of redissolved crystals show a clear sequence of peaks corresponding to the intact mixed-ligand cage with loss of increasing numbers of anions, but *no* peaks for the homoleptic cages which might also be expected. In other words, the mixed-ligand complex is the only product, even in solution, implying a cooperative interaction between the two types of ligand that renders formation of the mixed-ligand cage more favorable than formation of distinct homoleptic complexes with $L^{p\text{-}Ph}$ and L^{mes}.

With hindsight, one can see how the formation of this complex conforms to the simple requirement that the number of binding sites available from the ligand set must exactly match those required by the set of metal ions, and also that the spatial arrangement of ligand binding sites must match the stereoelectronic properties of the metal ions. This principle has been termed "avoidance of valence frustration" by Nitschke and coworkers [44]. Apart from that factor, which is important in all of the complexes described, the prediction that such an elaborate mixed-ligand assembly would form is clearly beyond our capabilities at the moment, particularly

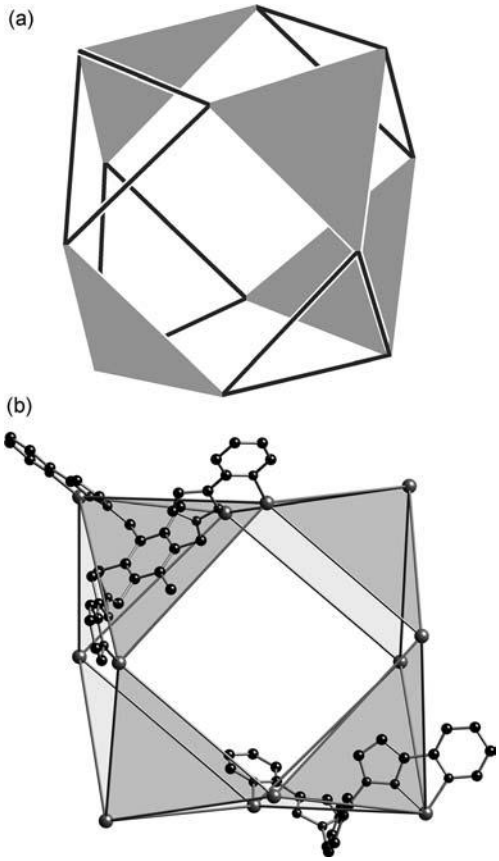

Figure 9.19 (a) A sketch of a cuboctahedron, showing how it can be delineated using four face capping ligands (shaded faces) and 12 edge-bridging ligands; (b) a view of the cuboctahedral metal core of $[Cu_{12}(\mu\text{-}L^{p\text{-}Ph})_{12}(\mu^3\text{-}L^{mes})_4](BF_4)_{24}$, which conforms to this principle (only one of each type of ligand is shown for clarity).

given the geometric flexibility of these ligands arising from the methylene spacers that were employed for synthetic convenience. Isolation of such beautiful cages must therefore – for the moment – rely to a large extent on serendipity. Having isolated them, however, the opportunities that they offer for studying properties such as host–guest chemistry and photophysical and chiroptical properties are extensive.

Acknowledgments

I am indebted to the many talented and patient research students and post-docs who have carried out this work; their names appear in the reference list. Financial support

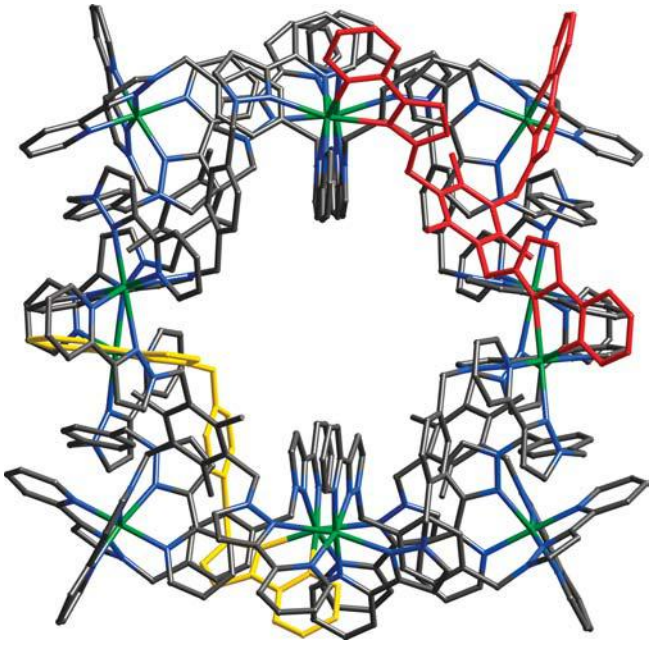

Figure 9.20 A view of $[Cu_{12}(\mu\text{-}L^{p\text{-}Ph})_{12}(\mu^3\text{-}L^{mes})_4](BF_4)_{24}$ showing all atoms in the cage, with one of the face-capping ligands of the bridging ligands colored red and one of the edge-bridging ligands colored yellow (Cu, green; N, blue).

from the EPSRC, the Leverhulme Trust and the Universities of Sheffield and Bristol is also gratefully acknowledged.

References

1 Lehn, J.-M., Rigault, A., Siegel, J., Harrowfield, J., Chevrier, B. and Moras, D. (1987) *Proc. Natl. Acad. Sci. USA*, **84**, 2565–2569.

2 Barley, M., Constable, E.C., Corr, S.A., McQueen, R.C.S., Nutkins, J.C., Ward, M.D. and Drew, M.G.B. (1988) *J. Chem. Soc., Dalton Trans.*, 2655–2662.

3 Youinou, M.-T., Rahmouni, N., Fischer, J. and Osborn, J.A. (1992) *Angew. Chem. Int. Ed. Engl.*, **31**, 733–735.

4 Baxter, P.N.W., Lehn, J.-M., Fischer, J. and Youinou, M.-T. (1994) *Angew. Chem. Int. Ed. Engl.*, **33**, 2284–2287.

5 Fiedler, D., Leung, D.H., Bergman, R.G. and Raymond, K.N. (2005) *Acc. Chem. Res.*, **38**, 349–358.

6 Fujita, M., Tominaga, M., Hori, A. and Therrien, B. (2005) *Acc. Chem. Res.*, **38**, 369–378.

7 Seidel, S.R. and Stang, P.J. (2002) *Acc. Chem. Res.*, **35**, 972–983.

8 Hasenknopf, B., Lehn, J.-M., Kneisel, B.O., Baum, G. and Fenske, D. (1996) *Angew. Chem. Int. Ed. Engl.*, **35**, 1838–1840.

9 Mamula, O., von Zelewsky, A. and Bernardinelli, G. (1996) *Angew. Chem. Int. Ed. Engl.*, **37**, 290–293.

10 Baxter, P.N.W., Lehn, J.-M., Baum, G. and Fenske, D. (1999) *Chem. Eur. J.*, **5**, 102–112.

11 Sauvage, J.-P. (1998) *Acc. Chem. Res.*, **31**, 611–619.

12 Fuller, A.M.L., Leigh, D.A., Lusby, P.J., Slawin, A.M.Z. and Walker, D.B. (2005) *J. Am. Chem. Soc.*, **127**, 12612–12619.

13 Dietrich-Buchecker, C., Colasson, B.X. and Sauvage, J.-P. (2005) *Top. Curr. Chem.*, **249**, 261–283.

14 Alvarez, S. (2005) *Dalton Trans.*, 2209–2233.

15 Rossmann, M.G., Arisaka, F., Battisti, A.J., Bowman, V.D., Chipman, P.R., Fokine, A., Hafenstein, S., Kanamaru, S., Kostyuchenko, V.A., Mesyanzhinov, V.V., Shneider, M.M., Morais, M.C., Leiman, P.G., Palermo, L.M., Parrish, C.R. and Xiao, C. (2007) *Acta Crystallogr., Sect. D*, **63**, 9–16.

16 Amoroso, A.J., Cargill Thompson, A.M.W., Jeffery, J.C., Jones, P.L., McCleverty, J.A. and Ward, M.D. (1994) *J. Chem. Soc., Chem. Commun.*, 2751–2752.

17 Bardwell, D.A., Jeffery, J.C., Jones, P.L., McCleverty, J.A., Psillakis, E., Reeves, Z. and Ward, M.D. (1997) *J. Chem. Soc., Dalton Trans.*, 2079–2086.

18 Armaroli, N., Accorsi, G., Barigelletti, F., Couchman, S.M., Fleming, J.S., Harden, N.C., Jeffery, J.C., Mann, K.L.V., McCleverty, J.A., Rees, L.H., Starling, S.R. and Ward, M.D. (1999) *Inorg. Chem.*, **38**, 5769–5776.

19 Jones, P.L., Byrom, K.J., Jeffery, J.C., McCleverty, J.A. and Ward, M.D. (1997) *Chem. Commun.*, 1361–1362.

20 Paul, R.L., Amoroso, A.J., Jones, P.L., Couchman, S.M., Reeves, Z.R., Rees, L.H., Jeffery, J.C., McCleverty, J.A. and Ward, M.D. (1999) *J. Chem. Soc., Dalton Trans.*, 1563–1568.

21 Amoroso, A.J., Jeffery, J.C., Jones, P.L., McCleverty, J.A., Thornton, P. and Ward, M.D. (1995) *Angew. Chem. Int. Ed. Engl.*, **34**, 1443–1446.

22 Fleming, J.S., Mann, K.L.V., Couchman, S.M., Jeffery, J.C., McCleverty, J.A. and Ward, M.D. (1998) *J. Chem. Soc., Dalton Trans.*, 2047–2052.

23 Fleming, J.S., Mann, K.L.V., Carraz, C.-A., Psillakis, E., Jeffery, J.C., McCleverty, J.A. and Ward, M.D. (1998) *Angew. Chem. Int. Ed.*, **37**, 1279–1281.

24 Paul, R.L., Bell, Z.R., Jeffery, J.C., McCleverty, J.A. and Ward, M.D. (2002) *Proc. Natl. Acad. Sci. USA*, **99**, 4883–4888.

25 Paul, R.L., Bell, Z.R., Jeffery, J.C., Harding, L.P., McCleverty, J.A. and Ward, M.D. (2003) *Polyhedron*, **22**, 781–787.

26 Frantz, R., Grange, C.S., Al-Rasbi, N.K., Ward, M.D. and Lacour, J. (2007) *Chem. Commun.*, 1459.

27 Argent, S.P., Riis-Johannessen, T., Jeffery, J.C., Harding, L.P. and Ward, M.D. (2005) *Chem. Commun.*, 4647–4649.

28 Al-Rasbi, N.K., Sabatini, C., Barigelletti, F. and Ward, M.D. (2006) *Dalton Trans.*, 4769–4772.

29 Bell, Z.R. and Ward, M.D. unpublished results.

30 Terpin, A.J., Ziegler, M., Johnson, D.W. and Raymond, K.N. (2001) *Angew. Chem. Int. Ed.*, **40**, 157.

31 http://www.webelements.com.

32 Paul, R.L., Argent, S.P., Jeffery, J.C., Harding, L.P., Lynam, J.M. and Ward, M.D. (2004) *Dalton Trans.*, 3453–3458.

33 Bell, Z.R., Harding, L.P. and Ward, M.D. (2003) *Chem. Commun.*, 2432–2433.

34 Argent, S.P., Adams, H., Harding, L.P. and Ward, M.D. (2006) *Dalton Trans.*, 542–544.

35 Bell, Z.R., Jeffery, J.C., McCleverty, J.A. and Ward, M.D. (2002) *Angew. Chem. Int. Ed.*, **41**, 2515–2518.

36 Argent, S.P., Adams, H., Riis-Johannessen, T., Jeffery, J.C., Harding, L.P., Mamula, O. and Ward, M.D. (2006) *Inorg. Chem.*, **45**, 3905–3919.

37 Argent, S.P., Adams, H., Riis-Johannessen, T., Jeffery, J.C., Harding, L.P. and Ward, M.D. (2006) *J. Am. Chem. Soc.*, **128**, 72–73.

38 Cotton, F.A., Murillo, C.A. and Yu, R. (2005) *Dalton Trans.*, 3161–3165.

39 Baxter, P.N.W., Lehn, J.-M., Baum, G. and Fenske, D. (1999) *Chem. Eur. J.*, **5**, 102–112.

40 Baxter, P.N.W., Lehn, J.-M., Kneisel, B.O. and Fenske, D. (1997) *Angew. Chem. Int. Ed. Engl.*, **36**, 1978–1981.

41 Ronson, T.K., Adams, H. and Ward, M.D. (2005) *Inorg. Chim. Acta*, **358**, 1943–1954.

42 Ronson, T.K., Adams, H., Riis-Johannessen, T., Jeffery, J.C. and Ward, M.D. (2006) *New J. Chem.*, **30**, 26–28.

43 Ward, M.D., McCleverty, J.A. and Jeffery, J.C. (2001) *Coord. Chem. Rev.*, **222**, 252–272.

44 Hutin, M., Bernardinelli, G. and Nitschke, J.R. (2006) *Proc. Natl. Acad. Sci. USA*, **103**, 17655–17660.

10
Periodic Nanostructures Based on Metal–Organic Frameworks (MOFs): En Route to Zeolite-like Metal–Organic Frameworks (ZMOFs)

Mohamed Eddaoudi and Jarrod F. Eubank

10.1
Introduction

The quest for solid-state materials possessing desired functionalities for specific applications is ever increasing. The discovery of novel functional materials or new functions for existing materials has been fundamental in their development for application processes, in addition to the advances in synthetic strategies towards such materials. However, the design of targeted functional solid-state materials for desired applications remains a scientific challenge [1]. In recent years, the successful introduction of new synthetic strategies, particularly the molecular building block (MBB) approach, has offered great potential for the eventual design of solid-state materials with targeted functions [2].

Porous or open-framework materials, such as zeolites and metal–organic assemblies (MOAs), are one of the most prominent groups of functional solid-state materials. They exhibit a broad range of properties that are ideal for critical applications, such as ion exchange, gas storage, separations or even catalysis [3,4], which depend greatly on the framework charge and composition, and also the shape and dimensions of the pores. The potential scope of natural and synthetic zeolites is well established; nevertheless, difficulties, such as expanding the pore size above the 1 nm prison and/or decorating the pores with organic functionalities, has restricted their application [5,6]. On the other hand, MOAs have burgeoned in recent years due, primarily, to their facile tunability (ease of modification), mild synthesis, multifunctional capacity and inorganic–organic hybrid nature [7], which allow the simple construction of functional materials, including zeolite-like metal–organic frameworks (ZMOFs), from myriad metal ion and organic linker combinations, to offer practically limitless properties for equally boundless applications.

Organic Nanostructures. Edited by Jerry L. Atwood and Jonathan W. Steed

ISBN: 978-3-527-31836-0

10.2
Historical Perspective

10.2.1
Metal–Cyanide Compounds

Metal–organic assemblies, themselves, are not new to the solid-state scientific community. As early as 1897, a nickel ammine cyanide compound was discovered by Hofmann and found to crystallize around benzene as $Ni(CN)_2{\cdot}NH_3{\cdot}C_6H_6$ [8,9]. Its ability to trap benzene led Hofmann to study the inclusion properties of this material, which indicated its selectivity for other small aromatic molecules depending on their size and shape [9,10]. Although a pivotal discovery, it was several years later before the crystal structure was solved for Hofmann's clathrate by Powell and Rayner [9,11]. They determined that the structure, $Ni(NH_3)_2Ni(CN)_4{\cdot}2C_6H_6$, was extended and consisted of alternating square-planar and octahedral Ni(II) cations bridged by cyanide anions, NiC_4 and NiN_6 (two axial ammonia molecules), resulting in layers of square grid sheets (Figure 10.1). The axial ammonia molecules are pointed into the interlayer spacing between sheets, where the benzene molecules are trapped perpendicular to the sheets.

Around the same time that Hofmann was developing his clathrates, interest in another type of metal–cyanide compound, Prussian blue (PB) and its analogues, also began to intensify [12]. Since its fortuitous discovery in 1704, the dye-related properties have resulted in numerous practical applications, which, combined with the discovery that the framework could be dehydrated while maintaining its structural integrity and could reversibly sorb small molecules, has attracted scientific interest in this class of metal–cyanide materials. As a result, there were many attempts to elucidate the chemical formula and metal oxidation state(s), including efforts to synthesize crystals for solid-state structure studies. It was not until 1970 that Prussian blue was determined to be a mixed-valence iron(III) hexacyanoferrate(II) compound and the first crystal structure was reported two years later, revealing a

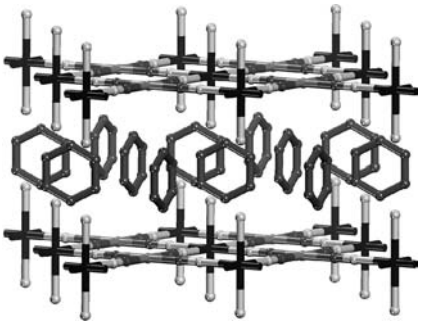

Figure 10.1 Crystal structure of Hofmann's clathrate. Hydrogen atoms have been omitted for clarity. Octahedral Ni = black, square-planar Ni = gray, C = dark gray and N = light gray.

Figure 10.2 Structure of Prussian blue. Hydrogen atoms have been omitted for clarity. Fe(III) = black, Fe(II) = dark gray, CN light gray and O = gray.

cubic structure with the general formula $Fe_4[Fe(CN)_6]_3{\cdot}xH_2O$ ($x = 14$–16), where defects in the structure are occupied by water molecules, resulting in $Fe^{II}C_6$ and $Fe^{III}N_{4.5}O_{1.5}$ coordination (Figure 10.2).

The unique host–guest properties and application potential of Hofmann's clathrates and Prussian blue have led to numerous attempts to target and construct analogous materials of each type. As with the MOAs of today, it was seen early on that these materials exhibited the potential for facile tunability based on substitution of the metal ions and/or organic ligands. Such substitutions would, no doubt, introduce novel properties to the materials while maintaining similar structural characteristics associated with each material type.

Specifically, the inclusion capability and selectivity of Hofmann's clathrate, along with the then newly known crystal structure, sparked interest in the development of similar materials. As early as the 1960s, researchers were attempting to substitute the Ni(II) ions with other metals [13], which eventually resulted in the development of a entire series of analogous compounds, aptly named Hofmann-type clathrates after their originator [14]. These Hofmann-type clathrates were then given the general formula $M(NH_3)_2M'(CN)_4{\cdot}2G$, where M = Cd, Co, Cu, Fe, Mn, Ni or Zn, M′ = Ni, Pd, Pt and G = C_4H_5N, C_4H_4S, C_6H_6 and $C_6H_5NH_2$ [14]. Further studies revealed that the square-planar M′ could be substituted with a tetrahedral metal ion, such as Cd or Hg [15], to give new three-dimensional metal–cyanide structures that were still capable of guest enclathration. Likewise, metal-substituted Prussian blue analogues were synthesized and have since been assigned the general formula $M_x[M'(CN)_6]_y$, including numerous transition metal, mixed transition metal and rare earth transition metal analogues with a range of properties, especially related to magnetism [12].

It has also been shown that other amine organic ligands could be utilized to modify the Hofmann-type structures by replacing the terminal ammonia ligands [9]. The most common of these alterations involves the use of diaminoalkanes, such as ethylenediamine ($NH_2CH_2CH_2NH_2$) and trimethylenediamine ($NH_2CH_2CH_2CH_2NH_2$) [12], which are ditopic ligands intended to replace two terminal ammonia ligands from neighboring metal–cyanide sheets, in effect pillaring the sheets and creating a 3D structure. In most cases the Hofmann-type metal–cyanide layers are maintained, merely the interlayer spacing and/or guest inclusion are altered. Longer diamines, $NH_2(CH_2)_nNH_2$ ($n = 4$–9), have been utilized to make modified Hofmann-type clathrates that can trap molecules larger than the typical small aromatic guests [12]. Although the metal–cyanide inclusion compounds can readily trap molecules, many are not stable upon loss of the guest molecules or heating [9,12]. There have been many efforts to synthesize more stable derivatives with unique properties or larger cavities, with limited success. The utilization of diaminoalkanes to pillar the Hofmann-type clathrate metal–cyanide sheets does add to their stability in some cases, but the ligands remain relatively flexible compared with the rigid cyanide bridges and can result in chelation of the metal instead of pillaring, and also collapse of the structure [9,12]. However, metal–cyanide chemistry has continued to progress with efforts to use rigid pillars, linear metal spacers [16] and even angular ditopic [17] or polytopic [18] amines to synthesize similar, and also unique [19], architectures. In addition, there have been numerous efforts to assess their potential for novel applications, including hydrogen storage [20].

10.2.2
Werner Complexes

Another series of solid-state organic–inorganic hybrid compounds that should not be overlooked are the Werner complexes (Figure 10.3), represented by the general formula MX_2A_4, where M = a divalent cation (Cd, Co, Cr, Cu, Fe, Hg, Mn, Ni, Zn) with octahedral coordination, X = an anionic ligand (Cl^-, Br^-, I^-, CN^-, NCO^-, NCS^-, NO_2^-, NO_3^-) and A = neutral pyridine-based ligands or α-arylalkylamines [21]. Like the Hofmann-type clathrates and Prussian blue-type materials, Werner complexes are inclusion compounds, having the ability to trap guest molecules due to the inefficient packing of the complexes in the solid state. The diversity of compositions allows for the inclusion of a variety of guest molecules, ranging from simple noble gases to complex aromatic molecules. The generality of the Werner complex formula, the scope of sorbed species and the occurrence of β-phases that exhibit porosity upon loss of guest molecules are indicative of the versatility of coordination chemistry and the utility of ligand substitution on the overall properties of metal–organic materials.

Although these Werner complexes and the previously mentioned metal–cyanide compounds have primarily focused on metals with octahedral coordination (and square planar in Hofmann-type clathrates), with few exceptions, it is evident that a variety of crystalline (periodic) inorganic–organic hybrid materials can be constructed. In addition, the dual composition of this class of materials offers the potential to alter

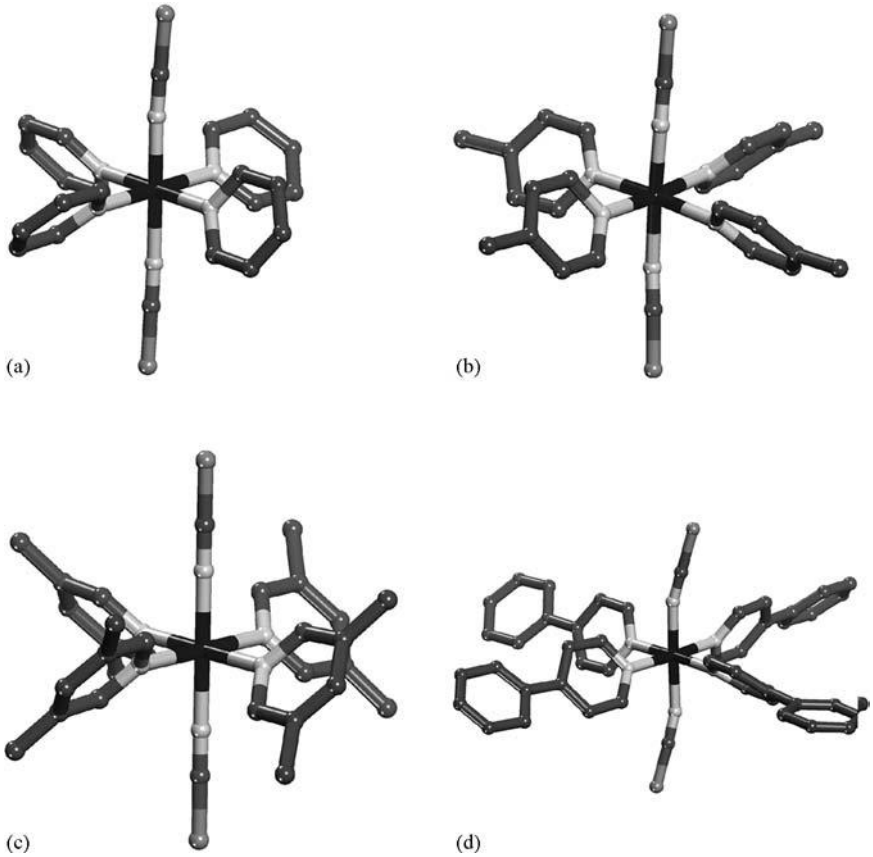

Figure 10.3 Typical MX_2A_4 Werner complexes: (a) X = NCS^-, A = pyridine; (b) X = NCS^-, A = 4-picoline; (c) X = NCS^-, A = 3,5-lutidine; and (d) X = NCS^-, A = 4-phenylpyridine.

the organic and inorganic components. Thus, the ability to introduce new coordination modes and geometries of metals, in combination with predesigned ligands, can only expand the scope and function of periodic hybrid materials.

10.2.3
Expanded Nitrogen-donor Ligands

However, it was not until 1989 that the potential for design was visualized and recognized for these inorganic–organic hybrid materials, when Hoskins and Robson first reported the deliberate design and synthesis of a cubic diamond-like MOA

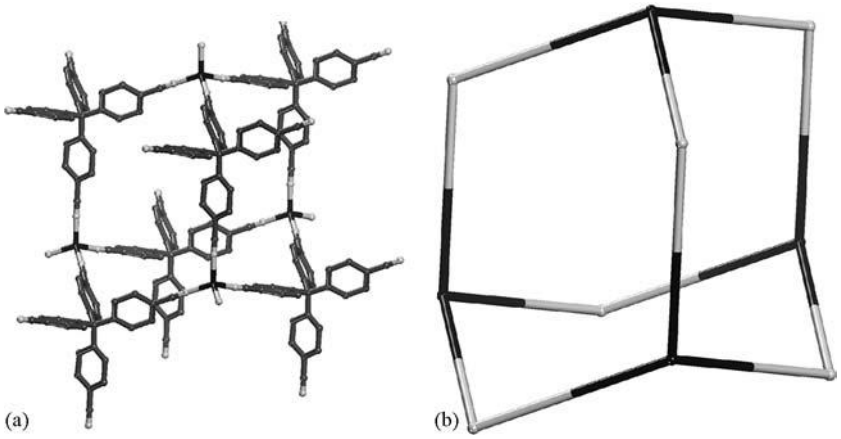

Figure 10.4 (a) Hoskins' and Robson's Cu-tetracyanotetraphenylmethane MOA (hydrogen atoms have been omitted for clarity; Cu = black, C = dark gray, N = light gray) with (b) cubic diamond topology.

constructed *in situ* from tetrahedral Cu(I) ions and 4,4′,4″,4‴-tetracyanotetraphenylmethane molecules (Figure 10.4) [22]. They proposed that if tetrahedral centers could be linked by molecular rods, an extended network could be constructed and expected to have an enlarged open structure related to cubic diamond or hexagonal Lonsdaleite that may be tailor-made (via variations in and modifications to the tetrahedral centers and molecular rods) to exhibit interesting properties. In a later publication, they elaborated on the subject, suggesting other possible molecular rods and coordination modes that might also be utilized to target particular frameworks, in addition to the potential for the resultant open materials to complement zeolites for related applications [23].

The hypotheses and results of Hoskins and Robson mark the beginnings of the molecular building block (MBB) approach, where the organic ligand and the metal ion each serve as building blocks *in situ*. These building blocks can then combine in numerous fashions to give a variety of architectures, depending on the size and shape of the organic linker and the coordination environment and geometry of the metal ion(s) [24]. These concepts opened the door to a new and interesting class of solid-state materials.

A variety of molecular rods could be utilized to target analogous and unique structures, but probably the most prominent example is 4,4′-bipyridine (bipy). Like the cyanide anion of the metal–cyanides mentioned previously, bipy can act as a linear ditopic ligand, possessing monodentate nitrogen donors at opposite ends of the molecule. The increased length of bipy, compared with cyanide, should result in larger cavities and thus more open structures.

The similarity of neutral bipy to the anionic cyanide linker suggests that structures with network topologies analogous to Hofmann-type clathrates could be targeted when coordinated to square-planar or octahedral metal ions in an MN_4 or MN_4L_2

fashion, respectively, where L = axial terminal ligands; octahedral MN_6 building blocks could lead to Prussian blue-type analogues. Indeed, the synthesis of materials consisting of layered square grid networks, like that of Hofmann-type clathrates, has been achieved by the combination of transition metal salts and bipy in various solvents, although anionic terminal ligands or guests are necessary to balance the charge of the cationic metals (i.e. neutral or cationic metal–bipy coordination polymers or frameworks) [25]. Likewise, cationic Prussion Blue-related octahedral assemblies have been synthesized from bipy and octahedral metal ions [26] and, as predicted, coordination to a tetrahedral metal center (MN_4) results in the formation of materials with frameworks related to the cubic diamond net [27].

In addition to structures composed of square grid sheets and linearly connected octahedra, a variety of networks have been synthesized from bipy and single metal ions depending on several factors, including the metal:ligand ratio, counter ions, guests and the coordination environment and geometry of the metal. Since bipy is a simple linear linker, the determination of each structure's network topology is directly governed by the coordination environment and geometry of the metal ion. A diversity of 3D structures can be targeted, including those analogous to the Si net in α-$ThSi_2$ [28], and also additional 2D [29,30], 1D [27,30,31] and discrete [32] topologies.

Other linear ditopic nitrogen-donor organic ligands (Figure 10.5), such as pyrazine, 1,2-bis(2-pyridyl)ethylene, 1,2-bis(4-pyridyl)ethane and many others, have

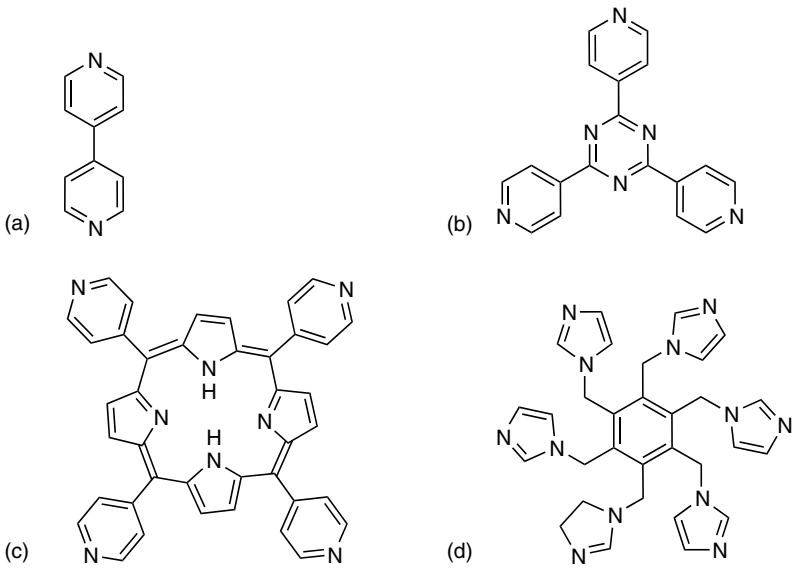

Figure 10.5 Nitrogen-donor organic ligands: (a) linear 4,4′-bipyridine; (b) 3-connector 2,4,6-tris(4-pyridyl)-1,3,5-triazine; (c) 4-connector 5,10,15,20-tetrakis(4-pyridyl)porphyrin; and (d) 6-connector 1,2,3,4,5,6-hexakis(imidazol-1-ylmethyl)benzene.

also been utilized to target compounds with analogous and novel topologies [33]. The coordination of these ligands to metal ions results in structures that have topologies ranging from discrete molecular squares [34] to 3D nets [35,36].

The success of the development of open metal–organic structures based on bipy-like ligands has led to the utilization of polytopic nitrogen-donor ligands for similar purposes. Although ditopic bipy merely serves as a linear spacer between metal ion nodes in the networks, other ditopic nitrogen donor ligands have been targeted with specific built-in angular nature to orient the metal ions at specific angles and target novel structures [37–39], including metal–organic frameworks with a sodalite-like topology [40]. In addition, nitrogen-donor ligands have been utilized with the potential to act as 3-, 4- or 6-connected linkers [41–43] (Figure 10.5). These non-linear ligands can then serve as additional nodes when coordinated to the metal ions, allowing for the synthesis of analogous and novel topologies when compared with bipy, depending on the size and shape of the ligand (limited only by the synthesis capabilities of the organic chemist) and the coordination environment and geometry of the metal ion [38].

Although recent developments have led to porous bipy-based MOAs [44], these materials typically remain unstable and collapse upon exchange or removal of guests and have been plagued by interpenetration [24]. Many of the bipy-like ligands are fairly rigid; however, lack of permanent porosity has traditionally been correlated with the flexible nature of the M–N coordination angles, which usually results in more flexible frameworks and limits their utility as porous materials [45].

10.2.4 Carboxylate-based Ligands

The quest for hybrid materials with large cavities and permanent porosity has led to the exploration for new coordination modes via carboxylate-based ligands to construct MOAs. Unlike the neutral bipy-like ligands, these anions can counter the cationic charge of the metal ions [45]. In addition, organic synthesis offers a vast repertoire of carboxylate-based ligands, many analogous in size and shape to the previously utilized nitrogen-donor molecules (Figure 10.6).

Due to the flexible nature of the monodentate coordination of nitrogen-donor ligands and, subsequently, the decreased predictability of the final structure, carboxylate ligands began to be explored as potentially multidentate moieties [24]. The ability of the carboxylate functionalities to bind metal ions in a bis-monodentate fashion (Figure 10.7) and form metal–carboxylate clusters has long been known [46], but only recently have researchers begun to target these clusters in the formation of extended MOAs from multi-carboxylate ligands [45].

Since they possess multiple metal–oxygen coordination bonds that result in the generation of rigid nodes with fixed geometry, these metal–carboxylate clusters are ideal molecular building blocks well suited for the construction of MOAs [45]. One of the most commonly used metal–carboxylate MBBs is the so-called paddlewheel cluster $[M_2(CO_2)_4L_2$, where L = ancillary ligands] [47]. This dinuclear MBB is

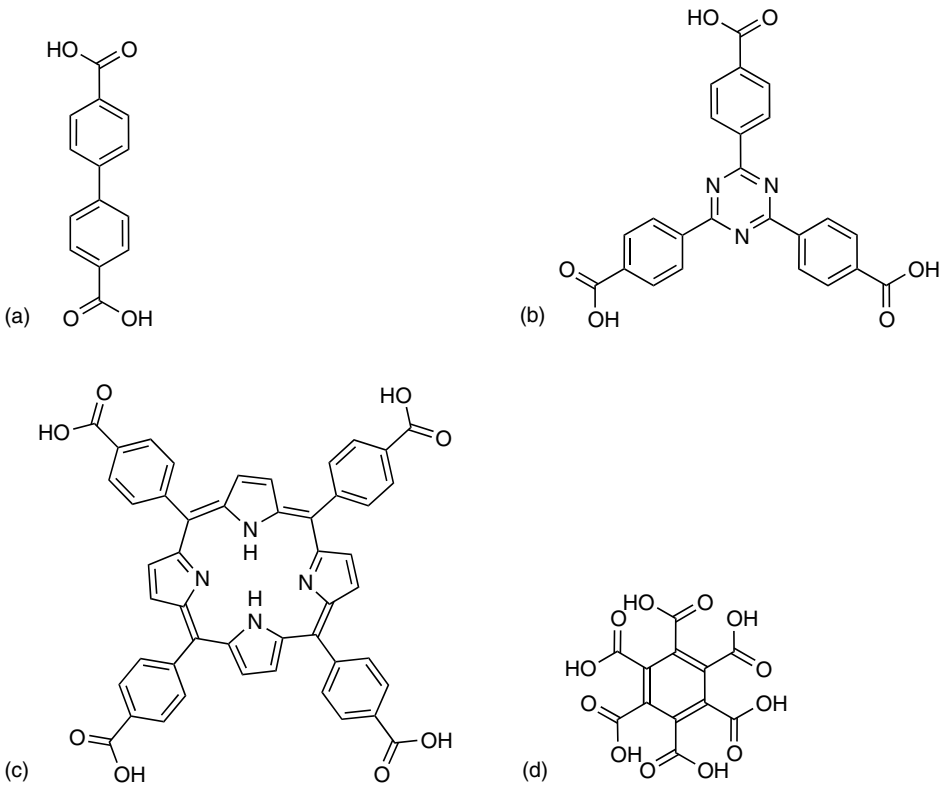

Figure 10.6 Carboxylate-based organic ligands: (a) linear 4,4′-biphenyldicarboxylic acid; (b) 3-connector 2,4,6-tris(4-carboxyphenyl)triazine; (c) 4-connector 5,10,15,20-tetrakis(4-carboxyphenyl)porphyrin; and (d) 6-connector mellitic acid.

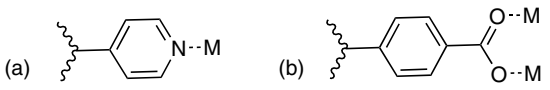

Figure 10.7 Common coordination modes in (a) bipy-like ligands and (b) carboxylate-based ligands.

most often targeted as a molecular square for building block purposes [7a,48,49] (Figure 10.8), but can be utilized as a linear spacer via the axial positions when equatorial carboxylates are terminal [48,49] or as an octahedral MBB if all the metal coordination sites are saturated with organic linkers [49]. However, there are a variety of other metal–carboxylate clusters that can be targeted as MBBs to construct stabile materials, including other dinuclear [50], trinuclear [$M_3O(CO_2)_6L_3$, basic

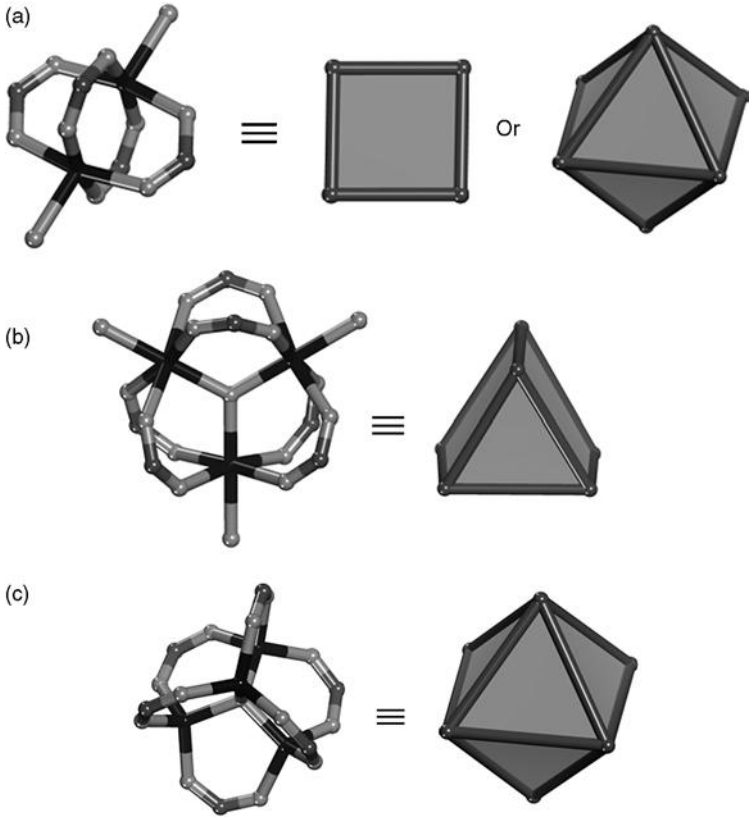

Figure 10.8 Common metal–carboxylate clusters and the resulting molecular building block(s): (a) paddlewheel can act as a linear (not shown), square or octahedral building block; (b) basic chromium acetate forms a trigonal prism building block; and (c) basic zinc acetate serves an octahedral building block.

chromium acetate] [51] and tetranuclear [$M_4O(CO_2)_6$, basic zinc acetate] clusters [52], through either ligand exchange or cluster generation *in situ*.

The ability to target, i.e. consistently generate *in situ*, these MBBs has attracted much attention since it provides the material designer with a prospective method to construct systematically functionalized porous materials. In general, if a given MBB can be targeted, the utilization of expanded or functionalized ligands can be used in conjunction with that MBB to construct analogous frameworks with varied pore size, shape and functionality [7c]. The viability and versatility of this metal–carboxylate approach has been proven many times over and has led to the burgeoning of this field when permanent porosity was finally achieved and proven for this class of materials in 1998 [53].

The metal–carboxylate cluster approach is exemplified through the basic zinc acetate MBB and its subsequent use in the construction of MOF-5 and numerous other extended CaB_6 analogues with unprecedented lower densities than encountered in any crystalline material [7b]. In addition, metal–carboxylate cluster MBBs have been utilized to synthesize homochiral MOFs for enantioselective separation and catalysis [51c]. Porous materials with some of the highest capacities for storage of carbon dioxide [54] and hydrogen [55] and the highest observed surface areas on any porous materials, up to about five times higher than the most open inorganic zeolite [51h,56]. In addition, rational synthesis of numerous MOAs [57] with various other predicted architectures [58,59] are on the rise. Although clear progress has been achieved in the design of MOAs using metal–carboxylates, the attainment of frameworks with default topologies is still predominant. Hence, new strategies are necessary to complement those already established in order to permit access to more complex structures.

10.3
Single-metal Ion-based Molecular Building Blocks

Combined with the desirable properties (inorganic–organic hybrid, mild synthesis, facile tunability and multifunctional capacity) and aesthetic architectures of the metal–organic materials themselves, the success of the MBB approach has promoted a surge not only in the synthesis of metal–organic assemblies, but also in the development of strategies toward the eventual design of desired functional porous materials for specific applications. As mentioned earlier, the utilization of metal–carboxylate clusters is one route to generate stability and target non-default structures, but methods that generate rigid MBBs from single-metal ions have not been realized. In the past, the use of single-metal ions and simple organic linkers as building blocks has consistently led to the construction of default structures depending on the shape(s) of the building blocks [57], which is supported by the synthesis of 2D square grid Hofmann-type clathrates and square grid and diamond nets from bipy-based ligands. These default structures are typically obtained due to the flexibility and lability of the (single-metal)–ligand coordination. Our group has recently developed and established a design strategy that involves a single-metal ion-based MBB approach that promotes the rational construction of atypical MOAs by forcing rigidity and directionality through control of the metal coordination sphere and judicious selection of suitable organic ligands [60].

Our group, among others, has utilized hetero-coordination of multifunctional organic molecules that combine both nitrogen donors and carboxylate groups with great success in the design and synthesis of novel functional materials [61], and our approach involves prior judicious selection of these would-be ligands based on the quantity and relative position of the functional groups on the molecule depending on the desired angle and target structure [60]. An aromatic ring must contain the nitrogen atoms and at least one nitrogen atom must have a carboxylic acid located

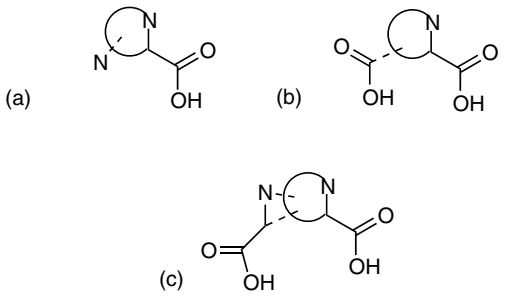

Figure 10.9 Possible variations of the $MN_{(x+y)}(CO_2)_{(x+z)}$ coordination, where M is any metal with coordination of 6–8, $x =$ number of *N,O*-hetero-chelating moieties, $y =$ the number of ancillary nitrogen-donors and $z =$ the number of ancillary carboxylic acids: (a) $x = 1$, $y = 1$, $z = 0$; (b) $x = 1$, $y = 0$, $z = 1$; (c) $x = 2$, $y = z = 0$. The ancillary group position depends on the desired angle and target structure.

one carbon away. This α-position allows for *N,O*-hetero-chelation to the metal ion. As part of the aromatic ring, the nitrogen atoms direct the framework topology, while the carboxylate groups secure the geometry of the metal by locking it into its position through the formation of rigid five-membered rings. In addition to having one hetero-chelating moiety, the organic molecule must also be polytopic, possessing at least one ancillary coordinating moiety, i.e. an additional carboxylate, nitrogen atom or hetero-chelate (Figure 10.9). The ability of a ligand to saturate the coordination sphere of the selected metal ion is also ideal, as this precludes coordination of any solvent, template or other guest molecules and allows directionality to be induced entirely dependent on the organic linker.

The use of potentially 6–8-coordinate metal ions allows the targeting of numerous structures, depending on the ligand shape and multiplicity of functionalities; this gives $MN_{(x+y)}(CO_2)_{(x+z)}$, where M is any metal with coordination of 6–8, $x =$ the number of *N,O*-hetero-chelating moieties, $y =$ the number of ancillary nitrogen-donors and $z =$ the number of ancillary carboxylic acids. Each hetero-coordinated single-metal ion can be rendered rigid and directional while simultaneously its coordination sphere is saturated via the coordination of the hetero-chelate and/or secondary functionalities of the ligands. The relative position of the ancillary functional group on the organic molecule dictates the directionality and plays a vital role in providing the angles necessary to target particular structures.

10.3.1
Discrete, 2D and 3D Metal–Organic Assemblies

Our design strategy has proven effective in synthesizing metal–organic polyhedra. The first example was a metal–organic cube using $Ni(NO_3)_2 \cdot 6H_2O$ and 4,5-imidazoledicarboxylic acid (H_3ImDC) [62]. H_3ImDC possesses concurrently the

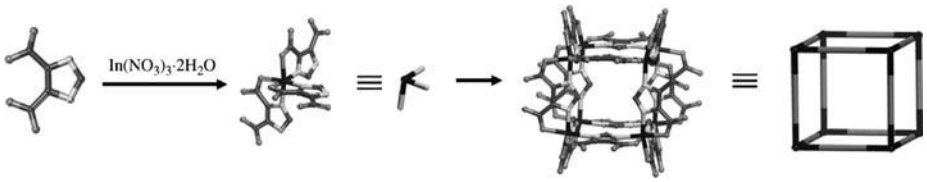

Figure 10.10 The metal–organic cube is constructed from 12 ImDC ligands and eight octahedral single-indium ion MBBs.

initial *N,O*-hetero-chelating moiety and an additional *N,O*-hetero-chelate. The H_3ImDC molecules are doubly deprotonated *in situ* and three $HImDC^{2-}$ anions coordinate each Ni^{2+} cation in a facial (*fac*) manner to complete the Ni(II) octahedral coordination sphere (Figure 10.10). Each ligand chelates two metal ions at a large angle, which allows the ligand to function as the edges of the cube while the *fac*-$NiN_3(CO_2)_3$ MBB occupies the vertices. As the metal–organic cube consists of 12 doubly deprotonated ligands and only eight divalent nickel ions, cationic amines used in the solvothermal synthesis conditions fill the inter-cube space and neutralize the anionic polyhedra, $[Ni_8(HImDC)_{12}]^{8-}\cdot[(H_2TMDP)_4]^{8+}\cdot(DMF)_4\cdot(EtOH)_4\cdot(H_2O)_6$.

The versatility of this approach was realized when we were able to synthesize supramolecular isomers using 2,5-pyridinedicarboxylic acid (H_2PDC) [63]. H_2PDC possesses concurrently the initial *N,O*-hetero-chelating moiety and an additional carboxylic acid in the 5-position, which can provide a 120° angle upon coordination. The angularity of this ligand can then be used to target discrete metal–organic octahedra or 2D metal–organic frameworks with Kagomé lattice topology, which are based on 4-connected vertices (Figure 10.11). Indeed, the H_2PDC molecules can be doubly deprotonated *in situ* and four PDC^{2-} anions can coordinate each metal cation [$MN_2(CO_2)_4$ MBB] to generate the 4-connected nodes necessary [$MN_2(CO_2)_2$

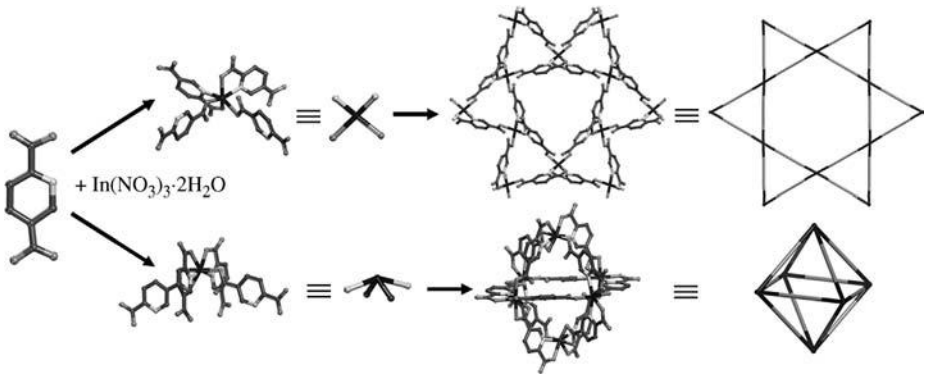

Figure 10.11 H_2PDC and $In(NO_3)_3\cdot 2H_2O$ were reacted in the presence of different SDAs to give a MOF with Kagomé lattice or metal–organic octahedra.

vertex]. As the coordination of four PDC^{2-} ligands to a single divalent or trivalent metal ion $\{[M^{II}(PDC)_4]^{2-}, [M^{III}(PDC)_4]^{1-}\}$ will yield an anionic framework, cationic structure directing agents (SDAs) can be utilized to direct the formation of the material.

In fact, the solvothermal reaction of H_2PDC and $In(NO_3)_3{\cdot}2H_2O$ in the presence of the SDA 4,4′-trimethylenedipiperidine (TMDP) yields a MOF with the Kagomé lattice topology, $[In(PDC)_2]_n^-{\cdot}(HTMDP)^+{\cdot}EtOH{\cdot}H_2O$ [63]. In this case, the single trivalent indium ions are 6-coordinate, each chelated by two ligands and coordinated through the ancillary carboxylates in a monodentate fashion by two additional ligands to give an $InN_2(CO_2)_4$ MBB, which can be simplified as a quasi-planar *cis*-$InN_2(CO_2)_2$ building unit. The anionic framework is neutralized by the protonation of the organic amine SDA, which occupies the hexagonal channels and interlayer space between the 2D Kagomé sheets along with guest solvent molecules.

The reaction of the same reactants in the presence of a different SDA, 1,2-diaminocyclohexane (DACH), results in the synthesis of an MOA consisting of discrete M_6L_{12} metal–organic octahedra and guests of the formula $[In_6(PDC)_{12}]^{6-}{\cdot}[(H_2DACH)_2]^{4+}{\cdot}[(H_3O)_2]^{2+}{\cdot}(DMF)_5{\cdot}(EtOH)_5$ [63]. Here, the single trivalent indium ions are actually 7-coordinate, each chelated by two ligands and one ancillary carboxylate in a monodentate fashion in the same manner as in the Kagomé lattice, but the ancillary carboxylate of one ligand binds in a bidentate fashion to the In(III) center. The coordination still gives an $InN_2(CO_2)_4$ MBB, as the points of extension are considered to be the carboxylate carbon atoms rather than the coordinated oxygen atoms, but the building unit is now quasi-pyramidal, *trans*-$InN_2(CO_2)_2$. As with the metal–organic cube, these polyhedra are anionic and the amine SDA molecules serve to neutralize the negative charge and actually link the octahedra together through N–H$\cdots$O hydrogen bonds to form a 3D network.

Thus, this method has proven effective in targeting and synthesizing discrete metal–organic polyhedra, metal–organic frameworks with Kagomé lattice topology and potentially 3D MOAs. One can envision using the same route to target other unique metal–organic assemblies from 6-, 7- or 8-coordinate single metal ions, including those with discrete, 2D and 3D architectures. Of great interest would be MOFs with zeolite-like topologies, due to the vast application potential of such materials associated with their porous and ionic nature.

10.3.2
Zeolite-like Metal–Organic Frameworks (ZMOFs)

Our single-metal ion-based MBB approach can also be applied to the decoration and/or expansion of tetrahedral-based zeolite-like nets [64] by lengthening the edges of the net with a longer functional organic linker [5,6], similar to the previously mentioned enlargement of metal–cyanide compounds by using an extended organic linker such as bipy. In effect, the organic ligand will serve as a functionalized multi-atom substitute for the single oxygen atoms that bridge the tetrahedral (T) silicon and/or aluminum atoms in traditional inorganic zeolites. However, the organic

ligand (L) must be judiciously selected to contain two functionalities (at least one *N,O*-hetero-chelate) that can provide an M–L–M angle comparable to the average T–O–T angle (~145°) found in typical zeolites [65]. In addition, higher coordination (6–8) metal ions are utilized instead of tetrahedral ions, so the ligands must coordinate to the metal in a manner that gives an MBB that can act as a tetrahedral building unit (TBU). Thus, for 6-coordinate metals there must be an $MN_4(CO_2)_2$ or $MN_2(CO_2)_4$ coordination environment and $MN_4(CO_2)_4$ or $MN_2(CO_2)_6$ MBBs for 8-coordinate metals that all result in MN_4 or $MN_2(CO_2)_2$ TBUs, respectively.

According to these criteria, the aforementioned organic molecule, H_3ImDC, is well suited to target metal–organic frameworks with zeolite-like topologies. This ligand concurrently possesses two *N,O*-hetero-chelating moieties with a potential M–L–M angle of 145°. When doubly deprotonated *in situ*, the $HImDC^{2-}$ anions can coordinate two divalent or trivalent metal cations at the appropriate angle (directed by the M–N coordination) and four ligands saturate each metal ion in the proposed manner to complete the respective coordination sphere and give an anionic zeolite-like metal–organic framework (ZMOF). This anionic nature allows for the utilization of different cationic SDAs and exploration of applications akin to inorganic zeolites.

As expected, solvothermal reaction of $In(NO_3)_3{\cdot}2H_2O$ and H_3ImDC in the presence of different SDAs yields metal–organic frameworks with different zeolite-like topologies, specifically *sod* (sodalite) and *rho* [59,65]. Predictably, the expansion of the oxygen atom bridge in existing zeolite topologies to the larger $HImDC^{2-}$ linker results in the two ZMOFs, *sod*-ZMOF and *rho*-ZMOF, that are up to eight times larger than their inorganic analogues. These new ZMOF materials offer great potential for numerous applications, combining the unique properties of both MOFs and zeolites, in addition to novel properties.

10.3.2.1 *sod*-ZMOF

The solvothermal reaction of H_2PDC and $In(NO_3)_3{\cdot}2H_2O$ in the presence of the imidazole (HIm) yields a MOF with a zeolite SOD-like topology, *sod*-ZMOF (Figure 10.12). In the crystal structure of *sod*-ZMOF, each single indium ion is chelated by two $HImDC^{2-}$ ligands and coordinated by the ancillary nitrogen donor of two more $HImDC^{2-}$ ligands, resulting in 6-coordinate In(III) ions that form $InN_4(CO_2)_2$ MBBs. Since the nitrogen atoms direct the topology, this MBB can be regarded as an InN_4 TBU. When the structure is reduced to the simplified InN_4 TBUs, it can be viewed a 3D periodic array of large truncated octahedral cages, analogous to β-cages found in numerous inorganic zeolites. These β-cages connect to neighboring cages through common four- and six-membered rings, which results in an overall structure based on the edge expansion of the inorganic sodalite net.

The presence of four $HImDC^{2-}$ ligands around each trivalent indium ion results in an anionic framework that is neutralized by the SDA molecules, $[In(HImDC)_2]_n^-{\cdot}[(H'HIm)]^+{\cdot}(DMF)_4{\cdot}(CH_3CN).(H_2O)_4$. Therefore, *sod*-ZMOF represents the first example of an MOF with an anionic framework based on the *sod* topology, although a few examples of neutral or cationic sodalite-like MOFs have been synthesized previously [57].

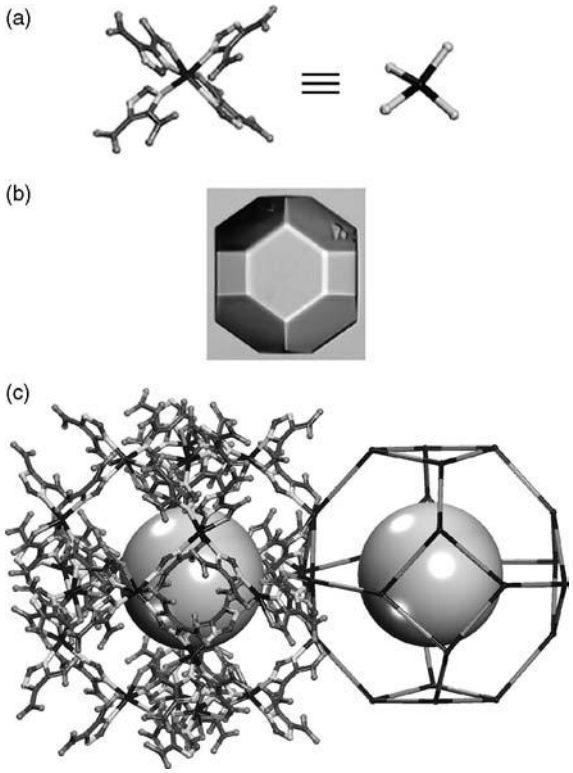

Figure 10.12 (a) *sod*-ZMOF is composed of 6-coordinated MBBs, which also can be viewed as 4-connected TBUs. (b) Optical image obtained on an Olympus MIC-D optical microscope of as-synthesized *sod*-ZMOF crystals. (c) A fragment of the *sod*-ZMOF single-crystal structure, where the large light-gray spheres represent the largest sphere that would fit in the β-cavities without touching the van der Waals atoms of the framework and the β-cages of the sodalite network connect through common four- (shown) and six-membered rings. Hydrogen atoms have been omitted for clarity; In = black, C = dark gray, O = gray, N = light gray.

10.3.2.2 *rho*-ZMOF

The same starting materials can be solvothermally reacted in the presence of a different SDA, 1,3,4,6,7,8-hexahydro-2*H*-pyrimido[1,2-*a*]pyrimidine (HPP), to yield a MOF with *rho* topology (Figure 10.13). In this case, each single indium ion is 8-coordinate, saturated by the chelation of four $HImDC^{2-}$ ligands to give $InN_4(CO_2)_4$ MBBs. As with *sod*-ZMOF, the nitrogen atoms of the ligand direct the topology and, although two additional α-carboxylates coordinate the metal ion, result in a 4-connected InN_4 TBU. When the structure is simplified as connected InN_4 TBUs, it is evident that four-, six- and eight-membered rings fuse together to form α-cages that are linked via double eight-membered rings (D8Rs) in a 3D periodic array to create first material ever to contain an organic component and have a zeolite *rho*-like topology [59]. The purity of the as-synthesized material

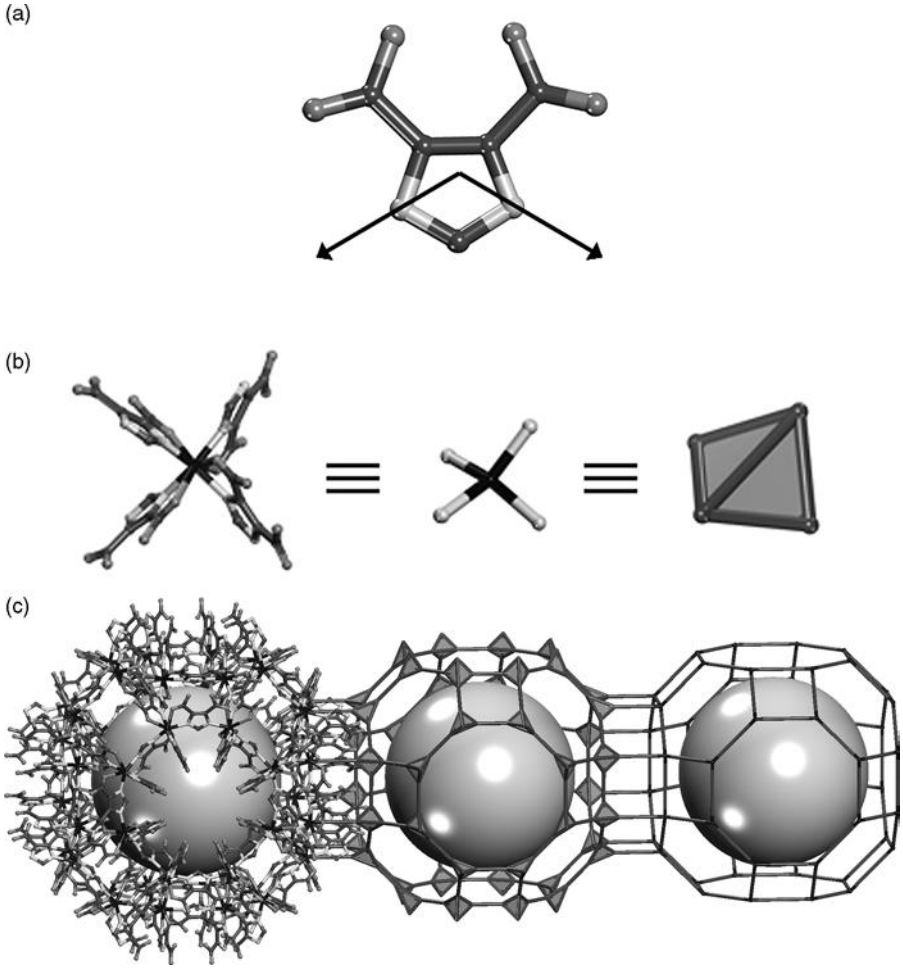

Figure 10.13 (a) The angle in the ImDC ligand. (b) *rho*-ZMOF is composed of 8-coordinated MBBs, which can be viewed as 4-connected TBUs. (c) A fragment of *rho*-ZMOF, where the large light-gray spheres represent the largest sphere that would fit in the α-cavities without touching the van der Waals atoms of the framework and the α-cages of the *rho* network connect through double eight-membered rings. Hydrogen atoms have been omitted for clarity; In = black, C = dark gray, O = gray, N = light gray.

was confirmed by similarities between the experimental and simulated XRPDs (Figure 10.14).

Again, the presence of four $HImDC^{2-}$ ligands around each trivalent indium ion results in the formation of an anionic framework that is neutralized by the SDA molecules, in this case 24 doubly protonated HPP molecules per unit cell, $[In_{48}(HImDC)_{96}]_n^{48-}\cdot[(H'_2HPP)_{24}]^{48+}\cdot(DMF)_{36}\cdot(H_2O)_{192}$. The H'_2HPP

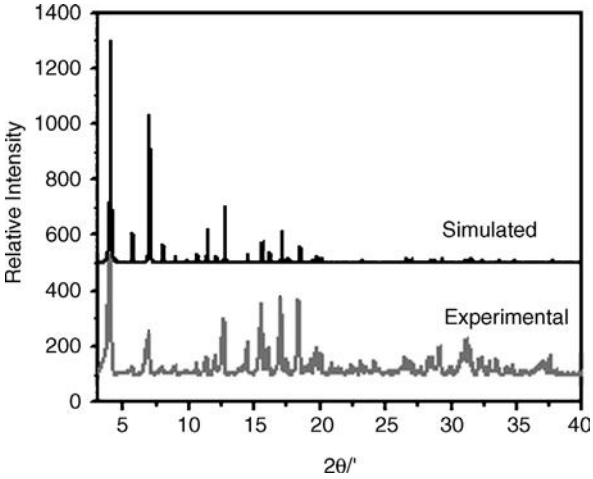

Figure 10.14 Experimental and simulated powder X-ray diffraction patterns for *rho*-ZMOF.

molecules occupy part of the open space in the α-cage cavities and the smaller D8R cages, in addition to the guest solvent molecules. The space occupied by guest molecules represents 56% of the cell volume or 16 718 $Å^3$ per unit cell and the as-synthesized compound is insoluble in water and common organic solvents.

The D8R cages of *rho*-ZMOF actually represent the largest apertures (~8 Å) of the framework for potential diffusion of small molecules. These pores serve as openings to the extra-large α-cage cavities, which have an internal diameter of 18.2 Å.

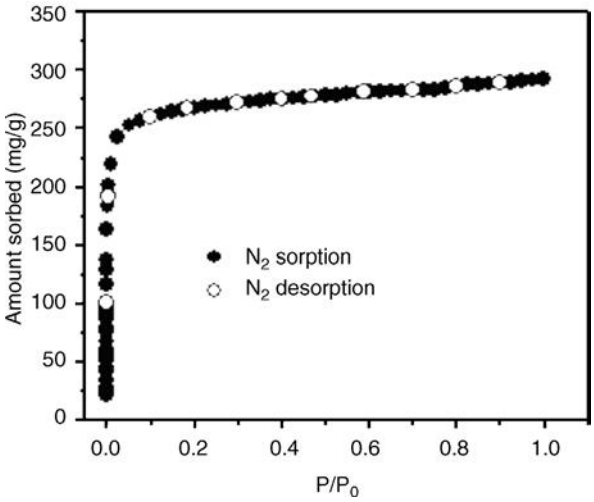

Figure 10.15 Nitrogen gas sorption isotherm for *rho*-ZMOF at 78 K.

The extra-large cavities and the anionic nature of *rho*-ZMOF make it ideal for applications involving cationic exchange, interesting considering that there are very few examples of anionic MOFs and the encapsulation of large molecules, an area where previous anionic porous materials, such as inorganic zeolites, have been limited [3].

Cation Exchange As stated previously, *rho*-ZMOF is an anionic framework; each α-cage is neutralized by 24 doubly protonated HPP molecules. In addition, the large apertures and robust nature (stable up to ~260 °C) of this material, suggest the potential to perform cationic exchange readily. Na^+ exchange can be achieved at

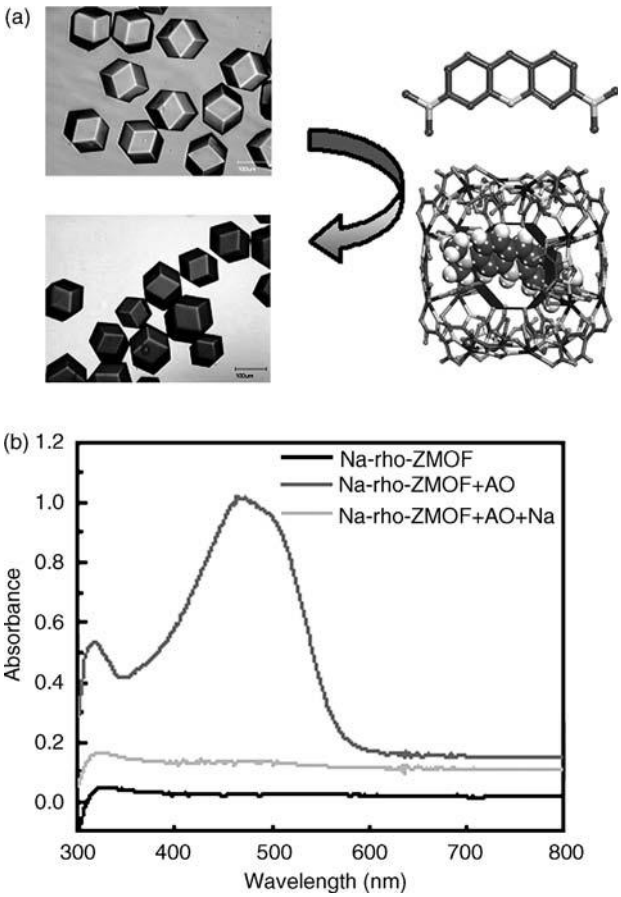

Figure 10.16 Optical images obtained on an Olympus MIC-D optical microscope of as-synthesized *rho*-ZMOF crystals (light gray = colorless) and *rho*-ZMOF crystals after AO exchange (dark gray = red) through the D8R windows. UV/Vis spectra of *rho*-ZMOF exchange derivatives.

room temperature, when 48 sodium ions replace the H'_2HPP molecules, which is confirmed by elemental microanalysis and atomic absorption studies. The crystallinity and structural integrity of *rho*-ZMOF are retained after Na^+ exchange, as indicated by similarities in the XRPD patterns. Cation exchange had never been successfully achieved in MOFs prior to this example, especially not in an aqueous environment, without dissociation of the framework [59].

The sodium-exchanged *rho*-ZMOF, Na-*rho*-ZMOF, can be fully evacuated at 100 °C, including guest water molecules. Sorption studies were conducted on the as-synthesized material and the sodium-exchanged derivative, revealing that both have type I nitrogen sorption isotherms (Figure 10.15). The isotherms are fully reversible, suggesting that the material contains homogeneous micropores; the apparent Langmuir surface area was estimated as $1067\,m^2\,g^{-1}$.

(Host–Guest)–Guest Sensing Just as Na^+ ions exchange cationic H'_2HPP molecules out of the *rho*-ZMOF cavities, other cationic organic molecules can also be utilized. There are numerous examples of cationic fluorophores, such as acridine orange (AO), which can be used to probe the physical properties of the *rho*-ZMOF interior. AO is also an excellent choice since it is smaller than the D8R aperture of *rho*-ZMOF and can diffuse freely into the α-cages (Figure 10.16).

The extra-large α-cage cavities allow not only the encapsulation of cationic molecules, but also additional neutral guest molecules. As AO is sensitive to its local environment, it can be utilized to sense a variety of neutral molecules, such as methylxanthines or DNA nucleoside bases. These results demonstrate the ability of anionic ZMOFs to serve as a (host–guest)–guest sensor with the ZMOF providing a periodic porous substrate for fluorescent cations which can then serve as the sensor unit.

10.4 Conclusion

Although serendipity will continue to aid in the advancement of science, the growing need for materials with specific functions will, no doubt, lead to an increased thrust for design strategies and methods. History has provided fundamental discoveries and principles that persist in modern solid-state materials development, such as the molecular building block approach. Our contribution has focused primarily on the utilization of single-metal ions as viable MBBs, depending upon the judicious selection of the organic ligands.

We have already proven the ability of this method to synthesize unique discrete, 2D and 3D metal–organic assemblies with targeted architectures, including the first anionic MOFs with zeolite-like topologies and properties, from higher coordination metals and ligands with specific angles and functionalities. One can envision how the single-metal ion-based MBB approach offers a rational route towards design and will, no doubt, aid the quest for novel functional materials.

References

1 (a) Robson, R., Abrahams, B.F., Batten, S.R., Gable, R.W., Hoskins, B.F. and Liu, J. (1992) *ACS Symp. Ser.*, **499**, 256–273. (b) Batten, S. R. and Robson, R. (1998) *Angew. Chem. Int. Ed.*, **37**, 1461–1494. (c) Champness, N.R. and Schroder, M. (1998) *Curr. Opin. Solid State Mater. Sci.*, **3**, 419–424. (d) Moulton, B. and Zaworotko, M.J. (2001) *Chem. Rev.*, **101**, 1629–1658. (e) Desiraju, G.R. (2003) *J. Molec. Struct.*, **656**, 5–15. (e) Rowsell, J.L.C. and Yaghi, O.M. (2004) *Microporous Mesoporous Mater.*, **73**, 3–14.

2 (a) Stein, A., Keller, S.W. and Mallouk, T.E. (1993) *Science*, **259**, 1558–1564. (b) Yaghi, O.M., Li, G. and Li, H. (1995) *Nature*, **378**, 703–706. (c) Pecoraro, V.L., Bodwin, J.J. and Cutland, A.D. (2000) *J. Solid State Chem.*, **152**, 68–77. (d) Holliday, B.J. and Mirkin, C.A. (2001) *Angew. Chem. Int. Ed.*, **40**, 2022–2043. (e) Pilkington, M. and Decurtins, S. (2003) *Perspect. Supramol. Chem.*, **7**, 275–323. (f) Finn, R.C., Burkholder, E. and Zubieta, J. (2003) *Perspect. Supramol. Chem.*, **7**, 241–274. (g) Brammer, L. (2004) *Chem. Soc. Rev.*, **33**, 476–489.

3 (a) Davis, M.E. (2002) *Nature*, **417**, 813–821. (b) Corma, A. and Davis, M.E. (2004) *Chem. Phys. Chem.*, **5**, 305–313.

4 (a) Kosal, M.E., Chou, J., Wilson, S.R. and Suslick, K.S. (2002) *Nat. Mater.*, **1**, 118–121. (b) Rowsell, J.L.C. and Yaghi, O.M. (2005) *Angew. Chem. Int. Ed.*, **44**, 4670–4679. Kaskel, S. (2005) *Nachr. Chem.*, **53**, 394–399. (c) Lin, W. (2005) *J. Solid State Chem.*, **178**, 2486–2490. (d) Mueller, U., Schubert, M., Teich, F., Puetter, H., Schierle-Arndt, K. and Pastre, J. (2006) *J. Mater. Chem.*, **16**, 626–636.

5 (a) Davis, M.E. (1997) *Chem. Eur. J.*, **3**, 1745–1750. (b) Jones, C.W., Katsuyuki, T. and Davis, M.E. (1998) *Nature*, **393**, 52–54. (c) Yamamoto, K., Sakata, Y., Nohara, Y., Takahashi, Y. and Tatsumi, T. (2003) *Science*, **300**, 470–472.

6 Cheetham, A.K., Férey, G. and Loiseau, T. (1999) *Angew. Chem. Int. Ed.*, **38**, 3268–3292.

7 (a) Eddaoudi, M., Moler, D.B., Li, H., Chen, B., Reineke, T.M., O'Keeffe, M. and Yaghi, O.M. (2001) *Acc. Chem. Res.*, **34**, 319–330. (b) Eddaoudi, M., Kim, J., Rosi, N., Vodak, D., Wachter, J., O'Keeffe, M. and Yaghi, O.M. (2002) *Science*, **295**, 469–472. (c) Yaghi, O.M., O'Keeffe, M., Ockwig, N.W., Chae, H.K., Eddaoudi, M. and Kim, J. (2003) *Nature*, **423**, 705–714.

8 Hofmann, K.A. and Küspert, F.A. (1897) *Z. Anorg. Chem.*, **15**, 204–207.

9 Iwamoto, T. (1984) in *Inclusion Compounds: Structural Aspects of Inclusion Compounds Formed by Inorganic and Organometallic Host Lattices*, **Vol. 1**, (eds J. L. Atwood, J.E.D. Davies and D.D. MacNicol), Academic Press, London, pp. 29–57.

10 (a) Hofmann, K.A. and Hochtlen, F. (1903) *Ber. Dtsch. Chem. Ges.*, **36**, 1149–1151. (b) Hofmann, K.A. and Arnoldi, H. (1906) *Ber. Dtsch. Chem. Ges.*, **39**, 339–344.

11 (a) Powell, H.M. and Rayner, J.H. (1949) *Nature*, **163**, 566–567. (b) Rayner, J.H. and Powell, H.M. (1952) *J. Chem. Soc.*, 319–328.

12 Dunbar, K.R. and Heintz, R.A. (1997) *Prog. Inorg. Chem.*, **45**, 283–391, and references therein.

13 Baur, R. and Schwarzenbach, G. (1960) *Helv. Chim. Acta*, **43**, 842–847.

14 Iwamoto, T., Nakano, T., Morita, M., Miyoshi, T., Miyamoto, T. and Sasaki, Y. (1968) *Inorg. Chim. Acta*, **2**, 313–316.

15 Iwamoto, T., Kiyoki, M., Ohtsu, Y. and Takeshige-Kato, Y. (1978) *Bull. Chem. Soc. Jpn.*, **51**, 488–491.

16 (a) Abrahams, B.F., Hardie, M.J., Hoskins, B.F., Robson, R. and Sutherland, E.E. (1994) *J. Chem. Soc. Chem. Commun.*, 1049–1050. (b) Soma, T., Yuge, H. and Iwamoto, T. (1994) *Angew. Chem. Int. Ed.*, **106**, 1746–1748. (c) Leznoff, D.B., Xue, B., Stevens, C.L., Storr, A., Thompson, R.C. and Patrick, B.O. (2001) *Polyhedron*, **20**, 1247–1254. (d) Niel, V., Munoz, M.C., Gaspar, A.B., Galet, A., Levchenko, G. and

Real, J.A. (2002) *Chem. Eur. J.*, **8**, 2446–2453.

17 (a) Niel, V., Galet, A., Gaspar, A.B., Munoz, M.C. and Real, J.A. (2003) *Chem. Commun.*, 1248–1249. (b) Niel, V., Thompson, A.L., Munoz, M.C., Galet, A., Goeta, A.E. and Real, J.A. (2003) *Angew. Chem. Int. Ed.*, **42**, 3760–3763.

18 (a) Abrahams, B.F., Hoskins, B.F., Liu, J. and Robson, R. (1991) *J. Am. Chem. Soc.*, **113**, 3045–3051. (b) Pickardt, J. and Gong, G.T. (1994) *Z. Anorg. Allg. Chem.*, **620**, 183–186.

19 (a) Abrahams, B.F., Hoskins, B.F. and Robson, R. (1990) *J. Chem. Soc. Chem. Commun.*, 60–61. (b) Gable, R.W., Hoskins, B.F. and Robson, R. (1990) *J. Chem. Soc. Chem. Commun.*, 762–763. (c) Batten, S.R., Hoskins, B.F. and Robson, R. (1991) *J. Chem. Soc. Chem. Commun.*, 445–447. (d) Hoskins, B.F., Robson, R. and Scarlett, N.V.Y. (1994) *J. Chem. Soc. Chem. Commun.*, 2025–2026. (e) Hoskins, B.F., Robson, R. and Scarlett, N.V.Y. (1995) *Angew. Chem. Int. Ed. Engl.*, **34**, 1203–1204.

20 Kaye, S.S. and Long, J.R. (2007) *Catal. Today*, **120**, 311–316, and references therein.

21 Lipowski, J. (1984) in *Inclusion Compounds: Structural Aspects of Inclusion Compounds Formed by Inorganic and Organometallic Host Lattices*, **Vol.1**, (eds J.L. Atwood, J.E.D. Davies and D.D. MacNicol), Academic Press, London, pp. 59–103, and references therein.

22 Hoskins, B.F. and Robson, R. (1989) *J. Am. Chem. Soc.*, **111**, 5962–5964.

23 Hoskins, B.F. and Robson, R. (1990) *J. Am. Chem. Soc.*, **112**, 1546–1554.

24 Yaghi, O.M., Li, H., Davis, C., Richardson, D. and Groy, T.L. (1998) *Acc. Chem. Res.*, **31**, 474–484.

25 Gable, R.W., Hoskins, B.F. and Robson, R. (1990) *J. Chem. Soc. Chem. Commun.*, 1677–1678. (b) Fujita, M., Kwon, Y.J., Washizu, S. and Ogura, K. (1994) *J. Am. Chem. Soc.*, **116**, 1151–1152. (c) Losier, P. and Zaworotko, M.J. (1997) *Angew. Chem. Int. Ed. Engl.*, **35**, 2779–2782. (d) Lu, J., Paliwala, T., Lim, S.C., Yu, C., Niu, T. and Jacobson, A.J. (1997) *Inorg. Chem.*, **36**, 923–929.

26 Subramanian, S. and Zaworotko, M.J. (1995) *Angew. Chem. Int. Ed. Engl.*, **34**, 2127–2129.

27 (a) MacGillivray, L.R., Subramanian, S. and Zaworotko, M.J. (1994) *J. Chem. Soc. Chem. Commun.*, 1325–1326. (b) Carlucci, L., Ciani, G., Prosperio, D.M. and Sironi, A. (1994) *J. Chem. Soc. Chem. Commun.*, 2755–2766. (c) Yaghi, O.M., Richardson, D.A., Li, G., Davis, C.E. and Groy, T.L. (1995) *Mater. Res. Soc. Symp. Proc.*, **371**, 15–19.

28 (a) Yaghi, O.M. and Li, H. (1995) *J. Am. Chem. Soc.*, **117**, 10401–10402. (b) Yaghi, O.M. and Li, H. (1996) *J. Am. Chem. Soc.*, **118**, 295–296.

29 Yaghi, O.M. and Li, H. (1995) *Angew. Chem. Int. Ed. Engl.*, **34**, 207–209.

30 Woodward, J.D., Backov, R.V., Abboud, K. A. and Talham, D.R. (2006) *Polyhedron*, **25**, 2605–2615.

31 Yaghi, O.M., Li, H. and Groy, T.L. (1997) *Inorg. Chem.*, **36**, 4292–4293.

32 Fujita, M., Yazaki, J. and Ogura, K. (1990) *J. Am. Chem. Soc.*, **112**, 5645–5647.

33 Kitagawa, S. and Kondo, M. (1998) *Bull. Chem. Soc. Jpn.*, **71**, 1739–1753.

34 Fujita, M. (1999) *Acc. Chem. Res.*, **32**, 53–61.

35 Power, K.N., Hennigar, T.L. and Zaworotko, M.J. (1998) *Chem. Commun.*, 595–596.

36 Carlucci, L., Ciani, G., Proserpio, D.M. and Sironi, A. (1995) *Angew. Chem. Int. Ed. Engl.*, **34**, 1895–1898.

37 Kaes, C., Katz, A. and Hosseini, M.W. (2000) *Chem. Rev.*, **100**, 3553–3590.

38 Leininger, S., Olenyuk, B. and Stang, P.J. (2000) *Chem. Rev.*, **100**, 853–908.

39 Navarro, J.A.R. and Lippert, B. (2001) *Coord. Chem. Rev.*, **222**, 219–250.

40 Tabares, L.C., Navarro, J.A.R. and Salas, J.M. (2001) *J. Am. Chem. Soc.*, **123**, 383–387.

41 3-Connected N-donor ligand: Fujita, M., Oguro, D., Miyazawa, M., Oka, H.,

Yamaguchi, K. and Ogura, K.((1995) *Nature*, **378**, 469–471. (b) Batten, S.R., Hoskins, B.F. and Robson, R. (1995) *Angew. Chem. Int. Ed. Engl.*, **34**, 820–822. (c) Batten, S.R., Hoskins, B.F. and Robson, R. (1995) *J. Am. Chem. Soc.*, **117**, 5385–5386. (d) Abrahams, B.F., Batten, S.R., Hamit, H., Hoskins, B.F. and Robson, R. (1996) *Chem. Commun.*, 1313–1314. (e) Abrahams, B.F., Batten, S.R., Hamit, H., Hoskins, B.F. and Robson, R. (1996) *Angew. Chem. Int. Ed. Engl.*, **35**, 1690–1692. (f) Ibukuro, F., Kusukawa, T. and Fujita, M. (1998) *J. Am. Chem. Soc.*, **120**, 8561–8562. (g) Abrahams, B.F., Batten, S. R., Grannas, M.J., Hamit, H., Hoskins, B. F. and Robson, R. (1999) *Angew. Chem. Int. Ed.*, **38**, 1475–1477

42 4-Connected N-donor ligand: Abrahams, B.F., Hoskins, B.F. and Robson, R. (1991) *J. Am. Chem. Soc.*, **113**, 3606–3607. (d) Abrahams, B.F., Hoskins, B.F., Michail, D.M. and Robson, R. (1994) *Nature*, **369**, 727–729. (c) Sharma, C.V.K., Broker, G.A., Huddleston, J.G., Baldwin, J.W., Metzger, R.M. and Rogers, R.D. (1999) *J. Am. Chem. Soc.*, **121**, 1137–1144. (d) Hagrman, D., Hagrman, P.J. and Zubieta, J. (1999) *Angew. Chem. Int. Ed.*, **38**, 3165–3168. (e) Kondo, M., Kimura, Y., Wada, K., Mizutani, T., Ito, Y. and Kitagawa, S. (2000) *Chem. Lett.*, 818–819.

43 6-Connected N-donor ligand:Hoskins, B.F., Robson, R. and Slizys, D.A. (1998) *Angew. Chem. Int. Ed.*, **36**, 2752–2755.

44 (a) Kondo, M., Yoshitomi, T., Seki, K., Matsuzaka, H. and Kitagawa, S. (1997) *Angew. Chem. Int. Ed. Engl.*, **36**, 1725–1727. (b) Ohmura, T., Usuki, A., Fukumori, K., Ohta, T., Ito, M. and Tatsumi, K. (2006) *Inorg. Chem.*, **45**, 7988–7990.

45 Eddaoudi, M., Li, H., Reineke, T.M., Fehr, M., Kelley, D.G., Groy, T.L. and Yaghi, O.M. (1999) *Top. Catal.*, **9**, 105–111.

46 (a) Watanabe, S. (1949) *Nature*, **163**, 225–226. (b) van Niekerk, J.N. and Schoening, F.R.L. (1953) *Nature*, **171**, 36–37. (c) van Niekerk, J.N. and Schoening, F.R.L. (1953) *Acta Crystallogr.*, **6**, 227–232. (d) van Niekerk, J.N., Schoening, F.R.L. and de Wet, J.F. (1953) *Acta Crystallogr.*, **6**, 501–504. (e) Koyama, H. and Saito, Y. (1954) *Bull. Chem. Soc. Jpn.*, **27**, 112–114.

47 Paddlewheel cluster; there are nearly 1800 occurrences in the Cambridge Structural Database (CSD) (January 2007): Allen, F. H. (2002) *Acta Crystallogr.*, **B58**, 380–388.

48 (a) Moulton, B., Lu, J., Hajndl, R., Hariharan, S. and Zaworotko, M.J. (2002) *Angew. Chem. Int. Ed.*, **41**, 2821–2824. (b) Eddaoudi, M., Kim, J., Vodak, D., Sudik, A., Wachter, J., O'Keeffe, M. and Yaghi, O.M. (2002) *Proc. Natl. Acad. Sci. USA*, **99**, 4900–4904. (c) Abourahma, H., Bodwell, G.J., Lu, J., Moulton, B., Pottie, I. R., Walsh, R.B. and Zaworotko, M.J. (2003) *Cryst. Growth Des.*, **3**, 513–519.

49 Cotton, F.A., Lin, C. and Murillo, C.A. (2001) *Acc. Chem. Res.*, **34**, 759–771.

50 Yaghi, O.M., Davis, C.E., Li, G. and Li, H. (1997) *J. Am. Chem. Soc.*, **119**, 2861–2868.

51 Basic chromium acetate trinuclear cluster; 385 occurrences in CSD [42]: Yaghi, O.M., Jernigan, R., Li, H., Davis, C.E. and Groy, T.L. (1997) *J. Chem. Soc. Dalton Trans.*, 2383–2384. (b) Li, H., Davis, C.E., Groy, T.L., Kelley, D.G. and Yaghi, O.M. (1998) *J. Am. Chem. Soc.*, **120**, 2186–2187. (c) Seo, J.S., Whang, D., Lee, H., Jun, S.I., Oh, J., Jin, Y. and Kim, K. (2000) *Nature*, **404**, 982–986. (d) Barthelet, K., Riou, D. and Férey, G. (2002) *Chem. Commun.*, 1492–1493. (e) Férey, G., Serre, C., Mellot-Draznieks, C., Millange, F., Surble, S., Dutour, J. and Margiolaki, I. (2004) *Angew. Chem. Int. Ed.*, **43**, 6296–6301. (f) Serre, C., Millange, F., Surble, S. and Férey, G. (2004) *Angew. Chem. Int. Ed.*, **43**, 6286–6289. (g) Sudik, A.C., Cote, A.P. and Yaghi, O.M. (2005) *Inorg. Chem.*, **44**, 2998–3000. (h) Férey, G., Mellot-Draznieks, C., Serre, C., Millange, F., Dutour, J., Surble, S. and Margiolaki, I. (2005) *Science*, **309**, 2040–2042. (i) Volkringer, C. and Loiseau, T. (2006) *Mater. Res. Bull.*, **41**, 948–954. (j) Ma, S., Wang, X., Manis, E.S., Collier, C.D. and Zhou, H. (2007) *Inorg. Chem.*, **46**,

3432–3434. (k) Liu, Y., Eubank, J.F., Cairns, A.J., Eckert, J., Kravtsov, V.Ch., Luebke, R. and Eddaoudi, M. (2007) *Angew. Chem. Int. Ed.*, **46**, 3278–3283.

52 Basic zinc acetate tetranuclear cluster; 18 occurrences in the CSD [42]: Li, H., Eddaoudi, M., O'Keeffe, M. and Yaghi, O. M. (1999) *Nature*, **402**, 276–279. (b) Kesanli, B., Cui, Y., Smith, M.R., Bittner, E.W., Bockrath, B.C. and Lin, W. (2005) *Angew. Chem. Int. Ed.*, **44**, 72–75. (c) Sun, D., Collins, D.J., Ke, Y., Zuo, J. and Zhou, H. (2006) *Chem. Eur. J.*, **12**, 3768–3776.

53 Li, H., Eddaoudi, M., Groy, T.L. and Yaghi, O.M. (1998) *J. Am. Chem. Soc.*, **120**, 8571–8572.

54 Millward, A.R. and Yaghi, O.M. (2005) *J. Am. Chem. Soc.*, **127**, 17998–17999.

55 Wong-Foy, A.G., Matzger, A.J. and Yaghi, O.M. (2006) *J. Am. Chem. Soc.*, **128**, 3494–3495.

56 Chae, H.K., Siberio-Perez, D.Y., Kim, J., Go, Y., Eddaoudi, M., Matzger, A.J., O'Keeffe, M. and Yaghi, O.M. (2004) *Nature*, **427**, 523–527.

57 Ockwig, N.W., Delgado-Friedrichs, O., O'Keeffe, M. and Yaghi, O.M. (2005) *Acc. Chem. Res.*, **38**, 176–182.

58 (a) Wells, A.F. (1977) *Three-Dimensional Nets and Polyhedra*, Wiley, New York. (b) Wells, A.F. (1979) *Further Studies of Three-Dimensional Nets*, American Crystallographic Association Monograph 8, American Crystallographic Association, Buffalo, NY. (c) O'Keeffe, M. and Hyde, B. G. (1996) *Crystal Structures I. Patterns and Symmetry*, Mineralogical Society of America, Washington, DC.

59 O'Keeffe, M. *Reticular Chemistry Structure Resource*, http://rcsr.anu.edu.au/.

60 Brant, J.A., Liu, Y., Sava, D.F., Beauchamp, D. and Eddaoudi, M. (2006) *J. Mol. Struct.*, **796**, 160–164.

61 (a) Eubank, J.F., Walsh, R.D. and Eddaoudi, M. (2005) *Chem. Commun.*, 2095–2097. (b) Eubank, J.F., Walsh, R.D., Poddar, P., Srikanth, H., Larsen, R.W. and Eddaoudi, M. (2006) *Cryst. Growth Des.*, **6**, 1453–1457.

62 Liu, Y., Kravtsov, V.Ch., Walsh, R.D., Poddar, P., Hariharan, S. and Eddaoudi, M. (2004) *Chem. Commun.*, 2828–2829.

63 Liu, Y., Kravtsov, V.Ch., Beauchamp, D.A., Eubank, J.F. and Eddaoudi, M. (2005) *J. Am. Chem. Soc.*, **127**, 7266–7267.

64 Liu, Y., Kravtsov, V.Ch., Larsen, R. and Eddaoudi, M. (2006) *Chem. Commun.*, 1488–1490.

65 Baerlocher, Ch. and McCusker, L.B. Database of Zeolite Structures http://iza-structure.org/databases/.